Journal of
Medicinal Chemistry

Article

Mechanistic insight on the mode of action of colletoic acid

Taotao Ling, Darcie J Miller, Walter Lang, Elizabeth Griffith, Adaris Rodríguez-Cortés, Ikbale El Ayachi, Gustavo Palacios, Jaeki Min, Gustavo A. Miranda-Carboni, Richard E Lee, and Fatima Rivas

J. Med. Chem., **Just Accepted Manuscript** • DOI: 10.1021/acs.jmedchem.9b00187 • Publication Date (Web): 11 Jul 2019

Just Accepted

is published by the American Chemical Society. 1155 Sixteenth Street N.W., Washington, DC 20036

Mechanistic Insight on the Mode of Action of Colletoic Acid

Taotao Ling,[‡] Darcie J. Miller,[ᵀ] Walter H. Lang,[‡] Elizabeth Griffith,[‡] Adaris Rodriguez-Cortes,[‡] Ikbale El Ayachi,[†] Gustavo Palacios,[‡] Jaeki Min,[‡] Gustavo Miranda-Carboni,[†] Richard E. Lee[‡] and Fatima Rivas[*,‡]*

[‡]Department of Chemical Biology and Therapeutics, [ᵀ]Department of Structural Biology, St. Jude Children's Research Hospital. 262 Danny Thomas Place. Memphis, TN 38105-3678, USA.[†]Department of Medicine, The University of Tennessee Health Science Center, Memphis, Tennessee 38163 USA.

ABSTRACT. The natural product colletoic acid (CA) is a selective inhibitor of 11β-hydroxysteroid dehydrogenase type 1 (11β-HSD1), which primarily converts cortisone to the active glucocorticoid (GC) cortisol. Here, CA's mode of action and its potential as a chemical tool to study intracellular GC signaling in adipogenesis is disclosed. 11β-HSD1 biochemical studies of CA indicated its functional groups at C-1, C-4, and C-9 were important for enzymatic activity; an X-ray crystal structure of 11β-HSD1 bound to CA at 2.6 Å resolution revealed the nature of those interactions, namely a close-fitting and favorable interactions between the constrained CA spirocycle, and the catalytic triad of 11β-HSD1. Structure-activity relationship studies culminated in the development of a superior CA analogue with improved target engagement. Furthermore, we demonstrate that CA selectively inhibits preadipocyte differentiation through 11β-HSD1 inhibition, suppressing other relevant key drivers of adipogenesis (i.e. PPARγ, PGC-1α), presumably by negatively modulating the glucocorticoid signaling pathway. The combined findings provide an in-depth evaluation of the mode of action of CA and its potential as a tool compound to study adipose tissue and its implications in metabolic syndrome.

INTRODUCTION

Intracellular cortisol levels are regulated by 11β-hydroxysteroid dehydrogenases 1 and 2 (11β-HSD), while circulating cortisol is controlled by the hypothalamic-pituitary-adrenal axis.[1-3] The present study focused on studying the correlation of the natural product (+)-colletoic acid (CA, **1**, Figure 1) with the bidirectional metabolic enzyme 11β-HSD1, which primarily activates local glucocorticoid (GC) action by converting cortisone to cortisol. 11β-HSD1 is highly expressed in metabolic tissue (i.e. adipose, liver),[4,5] and it can also exert context dependent regulation of cellular action in other tissue (muscle, osteoblast, etc.).[5] In humans, 11β-HSD1 expression is increased in acquired central obesity and positively correlates to accumulation of subcutaneous and intra-abdominal fat, body mass index, and insulin resistance, symptoms associated with metabolic syndrome (MetS) and type 2 diabetes mellitus (T2DM).[6-9] Inhibition of intracellular cortisol production by blocking 11β-HSD1 ameliorates the risk factors associated with MetS, T2DM, and fatty liver in preclinical studies.[6] Therefore, several medicinal chemistry campaigns have been launched to identify small heterocycle molecules to selectively inhibit 11β-HSD1.[10-14] However, the limited molecular complexity presented by heterocycles and the modest clinical performance have promoted the search for natural product inhibitors with rich structure complexity.[15] Despite the potential therapeutic relevance of this biological target, few natural products have been reported as potent and selective inhibitors of this enzyme (**3**-**4**, Figure 1).[16,17] For example, carbenoxolone (CBX, **4**) is a potent 11β-HSD1 inhibitor, but its poor isoform selectivity limits its use.[17]

Thus, natural products that can selectively inhibit 11β-HSD1 offer a unique opportunity to study intracellular GC signaling. Selective and tracktable 11β-HSD1 inhibitors can help improve our understanding of adipogenesis and its role in metabolic homeostasis, which is essential to develop new therapeutic avenues for the effective treatment of MetS, TDM2 and related disorders. Previous studies have demonstrated that CA is a potent 11β-HSD1 inhibitor with no observable 11β-HSD2 inhibition. [18, 19] CA is a member of the acorane natural products family, featuring a synthetically challenging all-carbon spirocenter. A convergent and enantioselective total synthesis of CA and its first-generation analogues were previously described by our group.[20] However, the exact mode of action of CA and its potential activity in functional cellular assays remained unknown. Thus, the main objective of our study was to elucidate the mode of action of CA and to develop new potential chemical tools to study GC signaling in adipocyte biology.

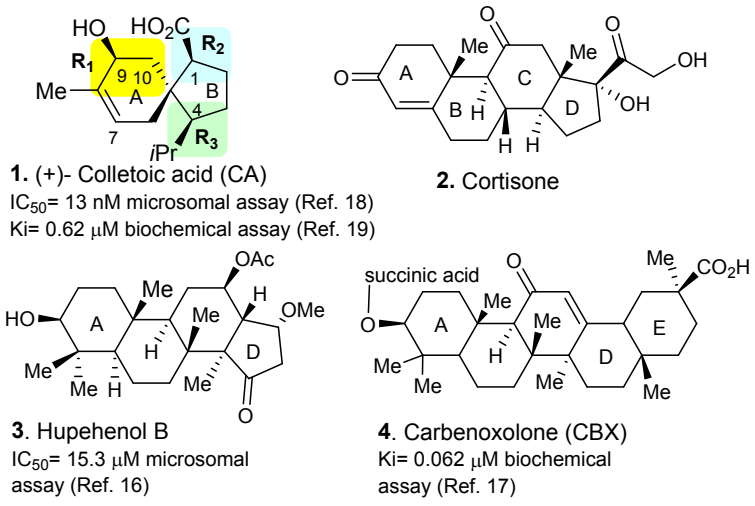

Figure 1. Representative natural product inhibitors of 11β-HSD1 and its native ligand.

Our streamlined synthetic strategy of the second generation of CA analogues successfully led to a superior 11β-HSD1 inhibitor, compound **20**. Simultaneously, we solved a single-crystal X-ray diffraction structure of the 11β-HSD1-CA complex, providing to the best of our knowledge, the first X-

ray structure of a selective and potent natural product inhibitor bound to this enzyme. Our study also provides novel insight into how CA inhibits preadipocyte differentiation via selective 11β-HSD1 inhibition in both murine and human preadipocytes cellular models. Through validation studies in the murine preadipocyte model, this work expands the current 11β-HSD1 pharmacological toolkit by providing a structurally distinct molecular scaffold, which can help explore the therapeutic potential of modulating intracellular GC action via 11β-HSD1 in adipose tissue.

RESULTS

Chemistry. Molecular docking studies of CA with 11β-HSD1 were performed prior to synthetic efforts, but provided limited information since the 11β-HSD1 cavity is flexible, and CA is relatively small (data not shown). Therefore, a systematic chemical modification of the core of CA was carried out to identify structure−activity relationship (SAR). The synthetic approach commenced with the total synthesis of the enantiomer of the natural product (+)-CA, (*ent*-**1**) to enable cross-validation studies of the combined chiral centers. It was envisioned that (−)-CA could arise from monoprotected 1, 3-cyclohexadione via a series of functional group manipulations, namely Wittig mono-olefination, acid-catalyzed ketone protection, deconjugation by treatment with DBU, hydrolysis of the ester followed by coupling with (*S*)-4-benzyl-2-oxazolidinone and alkylation with a vinyl iodide moiety at C-1, and a Heck-mediated cyclization reaction to afford the CA core system.[19] This synthetic effort provided *ent*-**1** in 19% yield over 21 steps from compound **21c** as a diastereomerically pure compound (Figure 2A). Next, to probe the influence of specific carbon centers (namely C-1, C-7 and C-8) of the natural product (+)-CA, several analogues were generated (Figure 2B). Initial efforts to direct amidation of the carboxylic acid under various conditions failed since rapid isomerization occurred at the C-1 center to yield the corresponding epimer. The resultant epimer is arranged in close proximity to the C-9 hydroxyl group, favorably facilitating an intramolecular nucleophilic cyclization to provide lactone **36** as the sole

product. To validate the identity of the epimer, base-mediated hydrolysis of lactone **36** was conducted, and compound **7** was isolated with no traces of (+)-CA. Esterification of CA with trimethylsilyldiazomethane in MeOH provided ester **5** in quantitative yield. Dihydroxylation of CA at C-7 and C-8 was achieved upon treatment with catalytic osmium tetroxide and NMO, yielding compound **12** in 82% yield as a single stereoisomer, presumably due to the C-9 hydroxyl group directing effect. However, the direct synthesis of the corresponding amide of CA, compound **6**, was prevented by this C-9 hydroxyl group. Thus, the C-9 hydroxyl group was oxidized with Dess–Martin periodinane, followed by treatment with ammonium salt and HATU in the presence of Hünig's base, providing compound **6** as a single diastereoisomer (at C-9) after enone reduction with sodium borohydride.

Subsequently, C-4, C-8, C-9 and C-10 centers of CA were evaluated (Figure 2C). Epoxide **13a** was synthesized from the CA core in gram quantity as previously reported,[20] which was subjected to a two-step reaction sequence involving Swern oxidation [$(COCl)_2$, DMSO, and Et_3N] of the primary hydroxyl group, followed by Pinnick oxidation ($NaClO_2$, *t*-BuOH, 2-Methyl-2-butene) to afford compound **13f**. Alternatively, compound **13a** was directly submitted to TBSCl in the presence of imidazole, and sequential treatment with thionyl chloride and pyridine at 0 ^oC to afford the exocyclic olefin system. Removal of the silyl group, and two-step oxidation of the primary alcohol resulted in compound **13e**. Acid-mediated epoxide opening occurred exclusively from the favored α-face and provided compound **13** in 81% yield. Then, the corresponding TBS-protected **13a** was treated with lithium aluminum hydride (LAH) at RT to provide a mixture of **10a** and **14a** in a 10:1 ratio. As expected, the aluminum ion coordinates with the C-8 hydroxyl group of compound **13a**, leading to hydride attack from the α-face, which yielded compound **10a** as the major product. Alternatively, reductive oxirane ring opening conditions (PtO_2/H_2) were used to obtain compound **14a** as the major product.[19] Compound **10a** was acetylated and exposed to two-step oxidation protocol (Swern/Pinnick), providing compound **11** in 77%

yield. Deprotection of the acetyl group followed by acid-promoted elimination led to the endocyclic compound **10**. Next, the C-9 hydroxyl group of **14a** was selectively protected with an acetyl group, as other evaluated protecting groups provided the thermodynamically more favorable endocyclic olefin during the elimination step. Then, the protected intermediate was treated with thionyl chloride, followed by TBAF to generate the exocyclic compound **14e**. Swern/Pinnick protocol provided compound **14**, followed by acetyl deprotection to afford compound **15** in 81% yield (Figure 2C). Finally, to evaluate the role of the substituent at C-4 and C-8, compounds **16i** and **20q** were generated. Following our synthetic streamlined protocol, compound **16i**, which was subjected to a series of protecting group maneuvers to selectively eliminate the tertiary hydroxyl group at C-8, and ultimately afford compound **16l**. The resultant compound was subjected to Swern/Pinnick oxidation and removal of the acetyl protecting group, afforded compound **16** in 59% overall yield from **16i**.

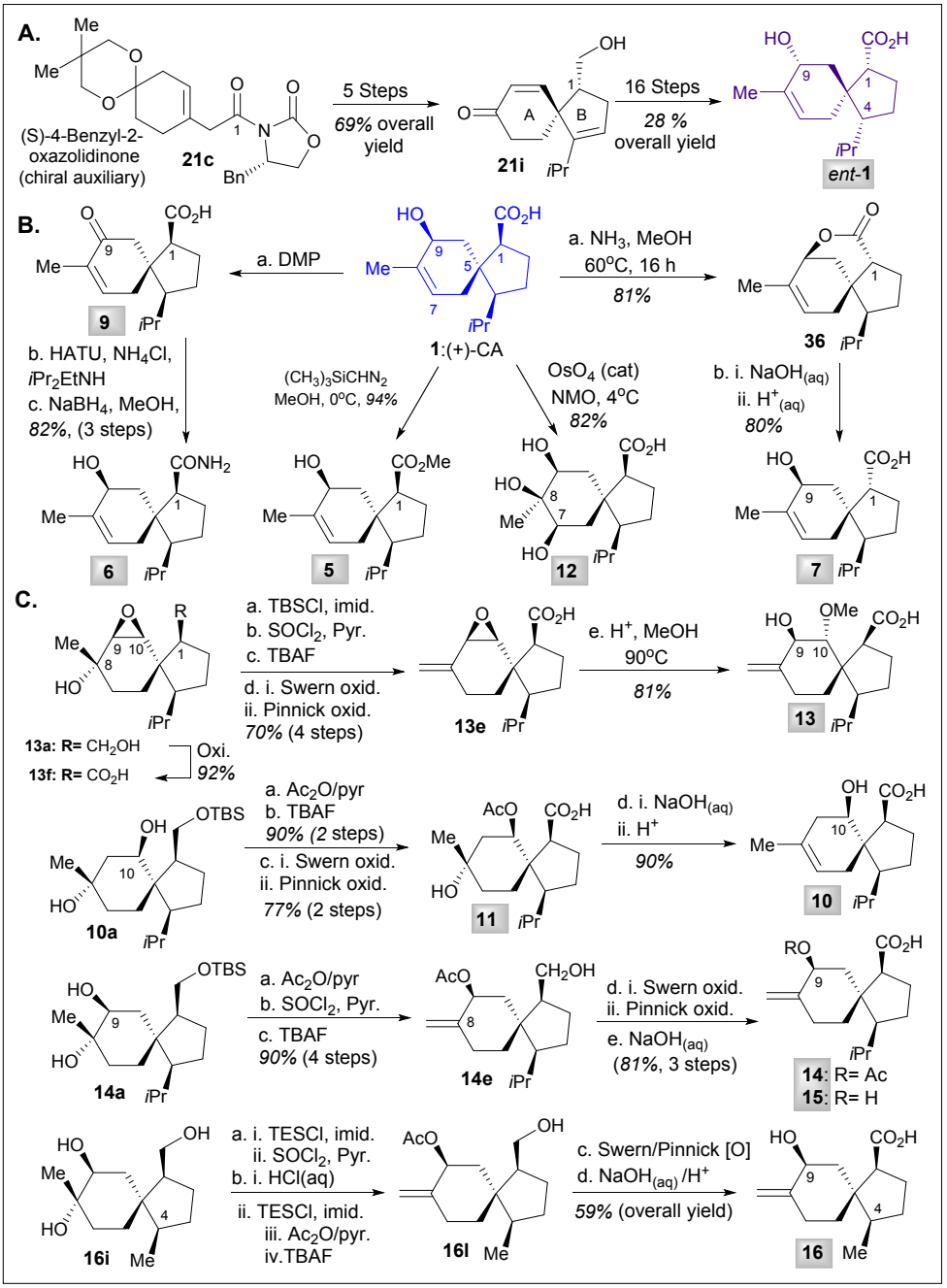

Figure 2. (A) Total synthesis of *ent*-**1**. (B) Synthesis of (+)-CA analogues derived directly from synthetic **1**. (C) Synthesis of CA analogues from advanced intermediates (Scheme S1-S5, Supporting Information).

Compounds **17**, **18** and **19** were the products of chemical transformations of compound **20o** (Figure 3). Olefin reduction and 1,2-opening of the epoxide **20o**, followed by protecting group maneuvers provided compound **20l** in 19% overall yield. Then 2-step oxidation of compound **20l**, followed by hydrolysis yielded compound **17** in 27% overall yield. Olefin reduction followed by 1,3 opening of the epoxide **20o** provided **20e** in good yield, which was mono-acetylated to afford compound **22ff** quantitatively. Thionyl chloride elimination followed by silyl protecting group removal leads to compound **22h**. Then 2-step oxidation of the corresponding free alcohol to the carboxylic acid, and consequent base treatment to remove the acetate group provided a mixture of compound **18** and **19** (2:1 ratio) in 85% overall yield. Finally, a series of chemical transformations and protecting group maneuvers were conducted upon compound **20q** to generate compound **20w** (in 19% overall yield), which was subjected to Swern/Pinnick protocol, followed by acetyl group deprotection, leading to compound **20** in 32% yield (3 steps).

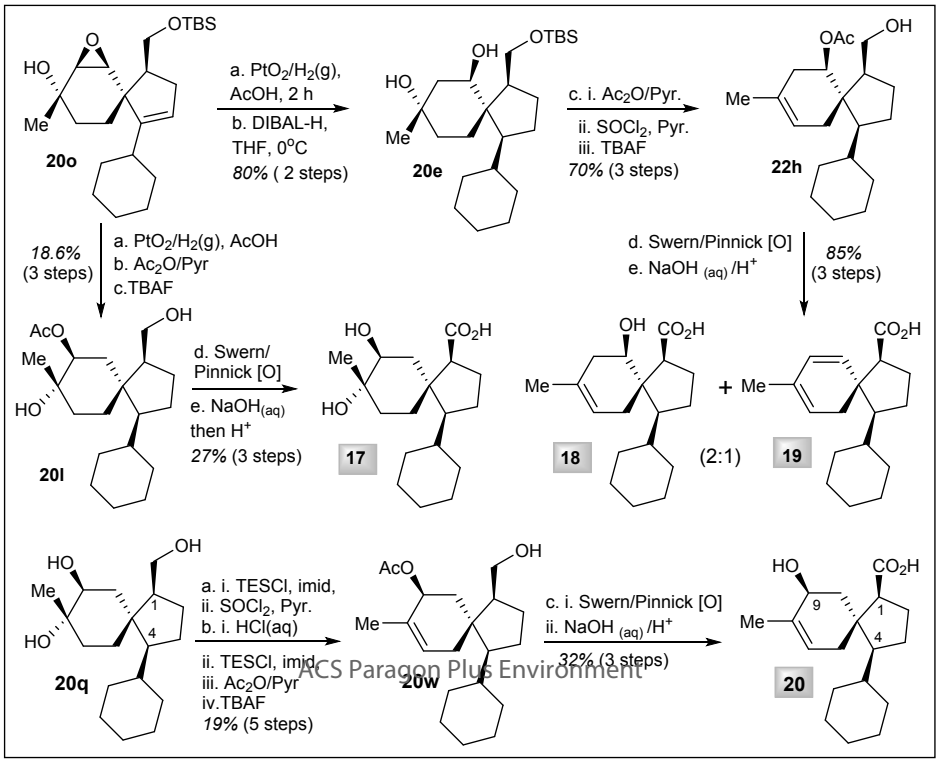

Figure 3. Synthesis of compounds **17-20** (Scheme S6, Supporting Information).

RESULTS AND DISCUSSION

Biochemical Evaluation of CA Analogues against Human 11β-HSD1. Although remarkable binding affinity results have been reported with enriched 11β-HSD1 microsomal assays by other groups,[21-23] variability among batches prompted us to work with a highly robust purified protein system measuring enzymatic activity as a function of cortisol concentration and NADPH fluorescence as a readout.[19, 22] Systematic SAR information was obtained by testing the generated CA analogues (Figure 4) using a biochemical assay with a truncated 11β-HSD1 construct to determine relative inhibition constant (K_i) values (Table 1). Based on these findings, and the intricate arrangement of functional groups of CA, it was anticipated that only (+)-CA (**1**), the natural enantiomer would have preference for engagement with the topology of 11β-HSD1 to form a lock-and-key fit. To validate this hypothesis, *ent*-**1** was synthesized and evaluated first, and it showed at least 30-fold decrease in activity when compared to (+)-CA as speculated. Next, the corresponding methyl ester **5** and amide **6** of CA were evaluated, and both compounds display weaker biochemical activity, indicating a potential important role for the carboxylic group at C-1. Compound **7**, the epimer of CA at C-1 showed significant loss of activity (K_i= 354 μM), highlighting the role of the carboxylic acid and its stereochemistry, which provide unique

diastereofacial features to CA. Next, the role of the C-9 hydroxyl group as a potential hydrogen donor was probed. Compound **8** with the acetylated hydroxyl group at C-9 displayed a decrease in activity (K_i= 21 μM). However, after oxidation of the C-9 hydroxyl group, the resulting compound **9** showed moderate activity (K_i= 5 μM). Evaluation of 3D molecular models of **9** indicated global conformational changes of the A ring (Figure S3, Supporting Information) induced by the restricting enone system, while this is a subtle change, the experimental data indicates a reduction in binding capacity to the enzyme. The analogue compound **10** bearing the hydroxyl group at C-10 showed modest potency, but its acetylated isomer **11**, also lacking the olefin, showed a significant decrease in activity, implying the hydroxyl group along with the conformation of the A ring play a role in the binding interactions with 11β-HSD1. Compound **12** was also less active than compound **10**. The sp3 hybridization at C-8 distorts the A ring, which adopts a twisted chair-like conformation in the *endo*-cyclic isomer, decreasing the productive engagement of carboxyl group at C-1 with the target. Next, the *exo*-cyclic system was interrogated by generating compounds **13**-**16**, in which the A ring adopts a chair conformation with the olefin in the pseudo equatorial position, while the C-9 substituent, and the carboxyl group are placed in a relative similar position as CA. Compound **13** with an additional group at C-10 (methoxy group) showed reduced activity, but in the same range as compound **12**. Compound **14** showed improved activity compared with compound **13**, presumably due to lack of the bulky methoxy group, which negatively affects the interactions required for the carboxylic group at C-1. Thus, compound **15** with the free C-9 hydroxyl group displayed better activity than compound **14** as it could interact with the catalytic triad similarly to CA. The combined findings indicate the carboxylic acid at C-1, the C-9 hydroxyl and the A ring conformation are important for effective binding to the target.

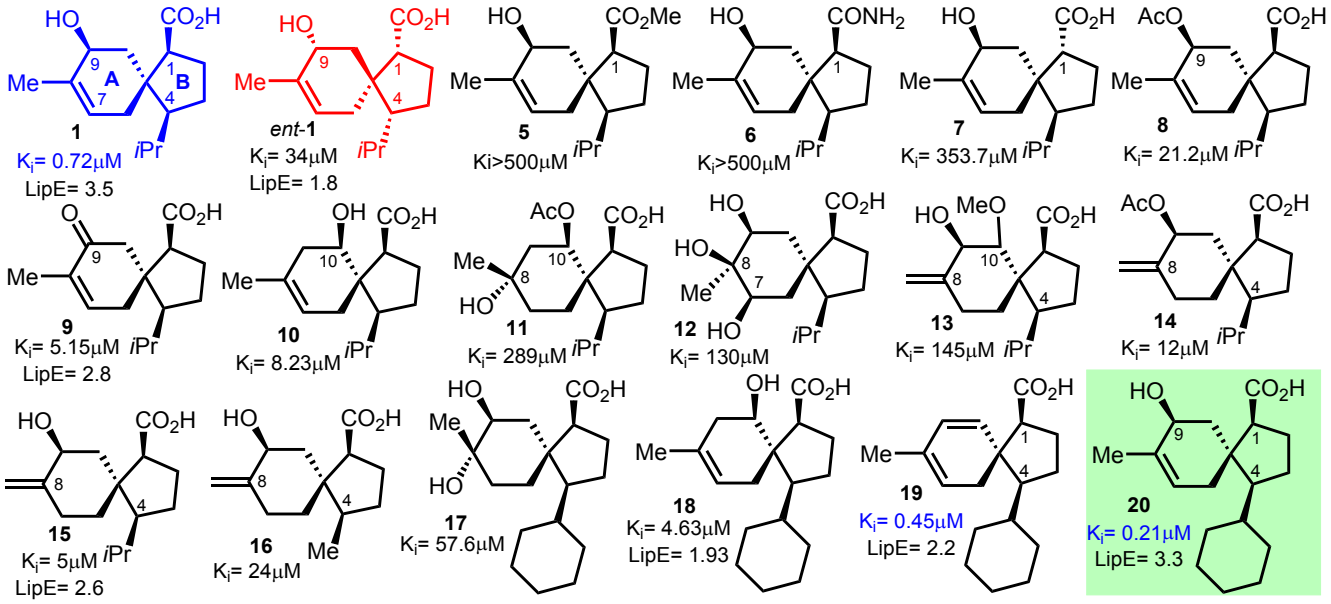

Figure 4. Biochemical activity (K_i) evaluation of CA analogues: SAR study.

Finally, the size of the substituent group at C-4 was investigated. Compound **16** displays a small methyl group substituent at C-4, exhibited five-fold less activity than compound **15**, indicating the isopropyl group was indeed also a contributing factor to the binding mode. This finding prompted us to hypothesize that a large hydrophobic group at C-4 might be involved in favorable hydrophobic interactions between the CA core and the binding site, and increase ligand residence time. Again, the sp3 nature of the C-8 was validated with compound **17** as it was weakly active, but compound **18** showed improved activity. Compounds **19** and **20** displayed further improved K_i values compared to CA. Gratifyingly, the superior compound **20** showed a three-fold increase of potency over CA.

Furthermore, these compounds (**1**, *ent-1*, **5-20**) showed selectivity for 11β-HSD1 over its isoform with no appreciable activity against 11β-HSD2 as shown in Table 1. The exquisite selectivity of these compounds is relevant as 11β-HSD2 inhibition can lead to hypertension, hyperinsulinemia among other side effects.[17] The work illustrates how small chemical modifications to the core of CA influence its binding ability, specifically, the presence and configuration of the carboxyl group at C-1, and the

influence of the hydroxyl groups at C-8, C-9, and C-10 on the conformational arrangement of the A ring. The linear chemical synthesis of CA enantiomer, C-1, C-4, and C-8 to C-10 chemical manipulations enabled a comprehensive SAR analysis against 11β-HSD1, leading to a superior CA analogue compound **20** (Figure 4). The combined biochemical and cytotoxicity data for CA and its analogues is described in Table 1, no cytotoxicity against the murine preadipocyte cell model (3T3-L1) under non-differentiating conditions was observed at the tested concentrations for these compounds.

Table 1. Biochemical and cytotoxicity evaluation of CA analogues.

Compound	11β-HSD1 Ki (μM)	11β-HSD1 IC_{50} (μM)	11β-HSD2 IC_{50} (μM)	3T3-L1 EC_{50} (μM)
1 (CA)	0.73 ± 0.26	4.1 ± 0.4	>500	>500
***ent*-1**	13.5 ± 2.2	80.3 ± 12.9	>500	>500
4 (CBX)	0.062 ± 0.038	0.41 ± 0.05	0.17± 0.05	>500
5	>500	>500	>500	>500
6	>500	>500	>500	>500
7	354 ± 194	>500	>500	>500
8	21.3 ± 4.4	178 ± 37	>500	>500
9	5.15± 0.30	42.4 ± 2.5	>500	>500
10	8.23± 0.63	55.1 ± 4.2	>500	>500
11	289 ± 58.4	>500	>500	>500
12	130 ± 57	>500	>500	>500
13	145 ± 23.5	>500	>500	>500
14	11.8 ± 1.9	71 ± 11.3	>500	>500
15	5.4 ± 0.47	38.3 ± 3.3	>500	>500
16	26.9 ± 4.8	162 ± 28.4	>500	>500
17	57.6 ± 5.4	379 ± 35.5	>500	>500
18	4.63± 0.57	27.2 ± 3.4	>500	>500
19	0.27 ± 0.034	2.2 ± 0.3	>500	>300
20	0.21 ± 0.022	1.34 ± 0.14	>500	>500
PF-915275	0.28 ± 0.058	2.07 ± 0.05	>500	23.55 ± 3.3

Target engagement: Complex of human 11β-HSD1 construct with CA. Based on previous 11β-HSD1 studies,[22, 24] it was hypothesized that CA would bind to the catalytic site as a competitive ligand. To test that hypothesis, co-crystallization and ligand-soaking strategies of CA with a construct of 11β-HSD1 containing the coding sequence for the catalytic domain (residues 24–292), a single point mutation (C272S), and a C-terminal truncation (residues 264–292) were conducted. These amino-acid perturbations of the protein construct are remote from the ligand- and cofactor-binding sites (the catalytic pocket) and should have minimum effects on the ligand-protein interaction as previously described.[19, 20] After several attempts, CA was soaked into pre-formed 11β-HSD1 crystals resulting in a 2.6-Å resolution structure of the 11β-HSD1-CA crystal complex (Table S3), with a root-mean-square deviation of 0.008 Å for aligned Cα atoms and describes the binding mode of CA to the enzyme for the first time. A global cartoon of the tetramer of 11β-HSD1 with CA bound near the cofactor NADP+ is shown in Figure 5, highlighting the narrow but flexible cavity of the ligand entrance.

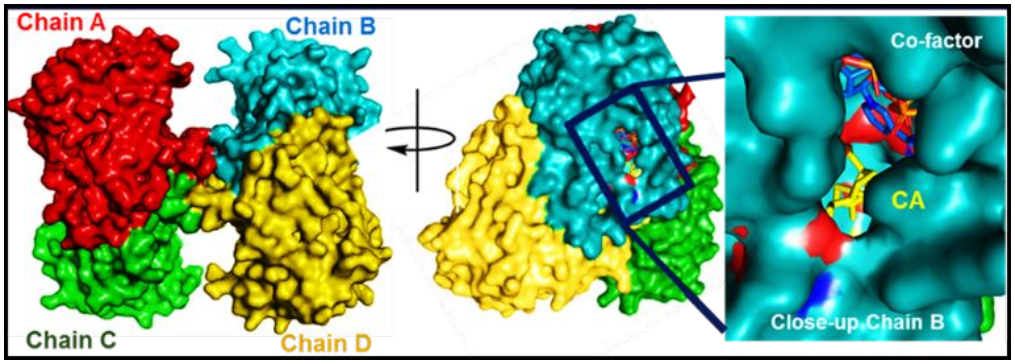

Figure 5. Cartoon model of the co-crystal structure of 11β-HSD1 tetramer with CA bound (6NJ7). The right panel provides a close-up view of the active site cavity surface for chain B with CA and NADP+ rendered as sticks (yellow for CA and dark blue for cofactor carbons, respectively).

The arrangement of the catalytic residues in the 11β-HSD1 active site align similar to previous reported crystal structures of 11β-HSD1, revealing a catalytic triad (Ser170, Tyr183, and Lys187) with a hydrophobic cavity that facilitates the interactions of steroidal chemical scaffolds.[22] The hydrophobic nature of the binding site and the conformational plasticity of 11β-HSD1 becomes evident when comparing open vs. closed states of the dimer with different ligands, clarifying why numerous small-molecule inhibitors with little or no structural similarities have been reported.[14] The substrate binding pocket of 11β-HSD1 is shielded from polar solvent as it is destined for hydrophobic substrates (cortisone/cortisol). The cofactor NADP+ binds to 11β-HSD1 analogous to previous reports[24] of binding at the active site, residing just above CA, in which the ribose rings display a C2-*endo* conformation. The nicotinamide ring of NADP+ is near the carboxylate of CA, and stabilization interactions occur because of the proximity.

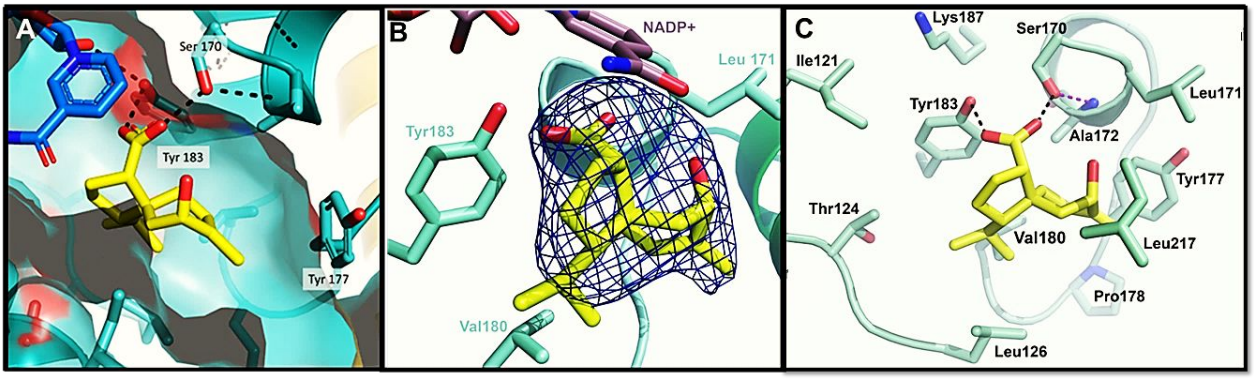

Figure 6. Close-up view of the crystal structure of the catalytic triad of 11β-HSD1 bound with CA as determined from collected co-crystal structure data (6NJ7). (A) CA (yellow) bound to 11β-HSD1 chain A, NADP+ is shown as dark blue. Hydrogen bonds are indicated by dashed lines. (B) Representative rendering of electron density of CA. (C) View looking down of the catalytic pocket (residues 226, 227, and 231 of the variable loop have been removed for clarity).

The ligand binding pocket is partially formed by the 'variable loop' and the C-terminal region of the dimer subunit, and this distal portion of the pocket is dynamic and is only partially observed within the crystal structure. The rigid anti-periplanar ring system of CA is fully appreciated in close-up images of the stick representation (Figure 6C), which highlights the rich stereo-complexity generated by the all-carbon spirocenter at C-5. The saturated five-membered B ring of CA, which can exist as a combination of puckered conformations, appears to favor the envelope conformer; it is unlikely to interconvert with the twist nonplanar form, which would require the simultaneous rearrangement of the cyclohexyl A ring, leading to an energetically unfavorable isomer. The carboxyl group at C-1 of CA interacts directly with both catalytic triad residues Tyr183 and Ser170, forming hydrogen bonds. Remarkably, the carboxylate moiety of CA also interacts with the cofactor NADP+: a highly favorable π-stacking interaction occurs between the negatively charged CA carboxylate and the positively charged nicotinamide moiety (Figure S4, Supporting Information). Furthermore, the hydroxyl group at C-9 of CA is close enough to form an intramolecular hydrogen bond with the carboxylate oxygen at C-1, potentially enhancing the stability of the bound inhibitor conformation. The methyl group at the C-8 position of CA is near the more-constrained region of the binding pocket, but there appears to be opportunities to introduce other functional groups at the C-8 that could favorably interact with Tyr 177 at the dimer interface. The electron density of the binding pocket complements the steric restrictions imposed by the compact scaffold of CA. The stereochemical disposition of the terminal methyl groups of the isopropyl group at C-4 are not clearly defined in the electron density, indicating freedom of rotation, which could accommodate larger hydrophobic groups. This unexpected finding was experimentally validated by compound **20** which shows superior inhibition (Table 1) due to the cyclohexyl group, suggesting that bulkier hydrophobic alkyl group can further improve the potency. Finally, the methyl groups were modelled in hydrophobic contact with the nonpolar residues Val180 and Leu126 due to its juxtaposition

as shown in Figure 6C, the predominantly hydrophobic amino acid residues that line the interface of the dimer become visible.

***In Vitro* Cellular Evaluation of CA.** The process of adipogenesis is highly regulated and it involves well-defined cellular stages, namely a commitment stage guided by transcription factors (such as CCAAT/enhancer-binding protein [C/EBP] family members, peroxisome proliferator-activated receptors, and glucocorticoid receptor) at the onset of differentiation, and cellular remodeling stage that is accompanied by lipid accumulation, leading to differentiation termination.[25-27] Hypertrophic growth involves the increase in size of the lipid droplet and an increase in protein content; such characteristics are exaggerated in obesity.[28-32] Several studies implicate GC signaling in both pre-adipocyte commitment during differentiation and hypertrophic adipocyte growth.[16] While 11β-HSD1 inhibitors have shown anti-diabetic effects *in vivo*,[12-14] such as PF-915275 and derivatives,[13] they also showed cytotoxicity against preadipocytes at the effective concentrations, presumably due to mitochondrial damage (Table S2, Supporting Information).[13b]

Thus, the adipogenesis cellular assay was selected to study and validate the biological activity of CA. First, the effects of CA on cell viability and cell cycle were evaluated in the murine 3T3-L1 preadipocyte model. CA showed no cytotoxicity at the tested concentrations (up to 1mM) with no significant effects on cell cycle under non-differentiating or induction conditions (Figure S7), rendering CA a valuable probe to study preadipocytes adipogenesis without cellular cytotoxicity. While we had previous shown that CA inhibits the conversion of [^{3}H]-cortisone to [^{3}H]-cortisol in the LPS activated murine J774.1 macrophage by inhibition of 11β-HSD1,[19] it was important to assess whether CA would also inhibit the glucocorticoid receptor (GR) signaling pathway via 11β-HSD1. In alignment to reported studies of glucocorticoid effects in 3T3-L1 differentiation by Kim, *et. al*.,[33a] dehydrocorticosterone (DHC), cortisone or dexamethasone were evaluated (Figure S7, Supporting Information). CA

significantly inhibits differentiation in the presence of all three compounds. For the presented successful differentiation of the cells, established protocols were followed.[33,34] For induction of the preadipocyte murine 3T3-L1 and human preadipocytes, dehydrocorticosterone or cortisone (250 nM), and hydrocortisone hemisuccinate (100 nM) were used respectively. Cells were treated with appropriate controls (non-differentiating medium NDM for negative control, differentiating medium with DMSO for positive control), or CA (50-100 μM) for 7 days for the murine cellular model, and 10-14 days for the human cellular model. Oil Red O staining (ORO) results of the 3T3-L1 cell model treated with negative control, positive control, or CA are shown in Figure 7 A-D respectively. CA treatment clearly inhibited adipogenesis when compared to the differentiated control cells, and showed a significant decrease in lipid droplet accumulation as quantified by ORO staining. A similar pattern of adipogenesis inhibition was observed for compound **20** as expected and at lower concentrations (Figure S11, Supporting Information). A neutral lipid (green) was used together with a mitochondria tracker (red) in a double staining experiment, providing a closer visualization of the cellular morphology and the lipid droplets at higher resolution (Figure 7 E-H). Unlike differentiated cells, CA treated cells displayed a staining pattern similar to undifferentiated cells. A significant ($p < 0.0001$) increase of lipid droplets was captured in those images for the positive control when compared to the negative control. However, for CA treated cells no significant difference was observed when compared to the NDM control cells. CA showed inhibition properties only when added at induction day. CA treatment after day 3 had little to no significant effect on the course of adipogenesis, indicating CA suppresses adipogenesis by attenuating GC signaling at the cell commitment stage. The adipocyte differentiation assay was also conducted with human visceral preadipocytes (Figure 7 I-L) and human subcutaneous preadipocyte (Figure S12, Supplemental Information). The cell doubling time is much slower, thus it took 10-14 days to observe significant lipid accumulation. CA also demonstrated modest inhibition of adipogenesis when compared

to the controls. However, the CA treated visceral human preadipocytes that differentiated displayed smaller lipid droplets than the corresponding differentiated control cells, indicating CA affected lipid accumulation. Interestingly, a greater effect was observed for the subcutaneous preadipocytes than for the visceral preadipocytes. Also, no quantifiable effect was observed in human preadipocytes when CA was added at day 3 after induction, highlighting the adipogenesis inhibitory effects on early stage cell-fate commitment.

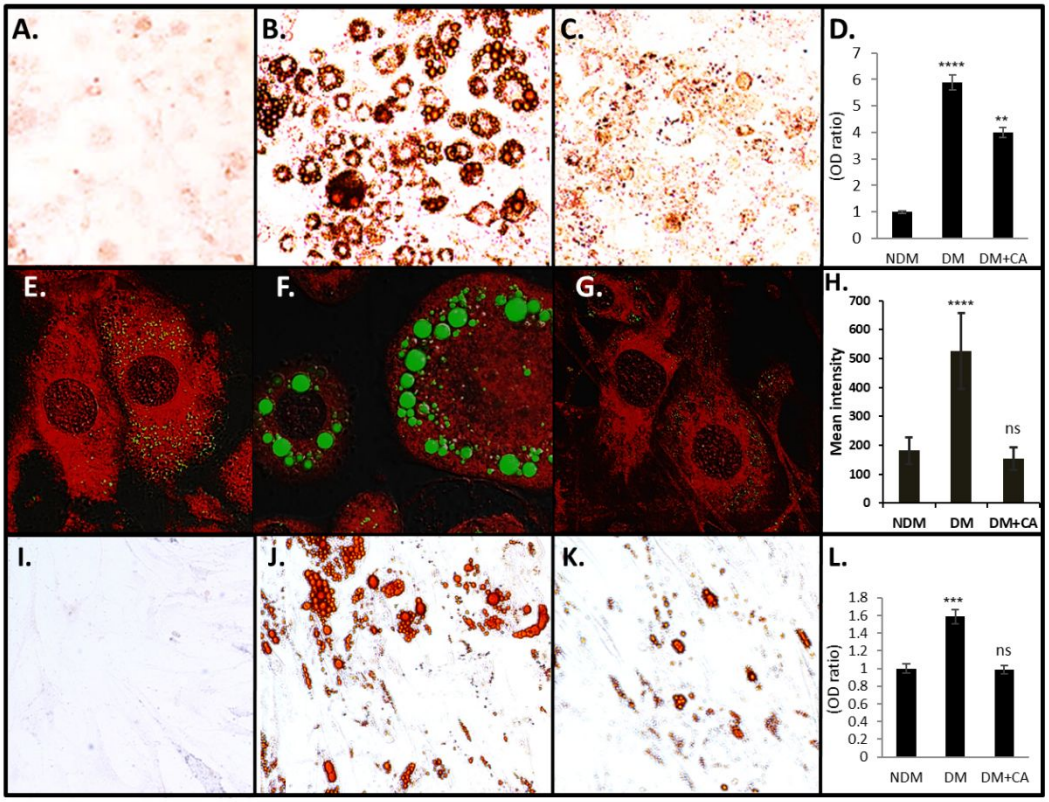

Figure 7. Representative images of adipogenesis assay of murine 3T3-L1 (A-H), and visceral human preadipocytes (I-L) after staining with Oil Red O (red) or lipid stain (green along with mitochondria red tracker). (A and I) Non-differentiating medium (NDM)–treated control cells. (B and J) Differentiating medium (DM)–treated control cells. (C and K) DM and CA (50 μM)-treated cells. (D and L) Relative quantification of ORO. (E) NDM–treated control cells. (F) DM–treated control cells. (G) DM and CA (50 μM)-treated cells. (H) Relative Mean FL intensity of lipid staining (green). Magnification 10× in A-C and I-K, and 63× in E-G.

Next, the steady-state gene transcript levels relevant to the adipogenesis process were measured for 3T3-L1 by using qRT-PCR, and the effects of CA inhibition on cell-fate and fatty acid accumulation related genes for days 0, 1, 2, and 7 was determined (Figure 8).[35] First CREB, C/EBP isoforms (α, β, δ), and S6K1 were evaluated as they are crucially involved in the early stage of adipocyte differentiation. Upon induction of adipocyte differentiation, phosphorylation of CREB leads to activation of C/EBP transcription, and an increase in C/EBPα, β and δ mRNA levels is expected. Indeed, a modest increase of the mRNA level of these genes was observed on day 1 and day 2 in the control differentiated cells, while CA-treated cells showed a significant reduction of C/EBPα, β and δ mRNA expression for day 1-2, namely during induction, the critical period that determines cell-fate. A similar mRNA expression reduction was recorded for the S6K1 gene for the CA-treated cells at day 1 and day 2. S6K1 has been described as a key element of adipocyte differentiation commitment.[36] During later stage of adipocyte differentiation, Peroxisome Proliferator-activated Receptor γ (PPARγ) and PPARγ coactivator-1-alpha (PGC-1α) promote accumulation of fatty acid deposits, leading to visible lipid dropplets.[37-38] In the differentiated 3T3-L1 cells, mRNA expression levels of these genes were significantly elevated by day 2

and plateau at day 7 (Figure 8). However, the mRNA expression level of the same genes was greatly reduced in CA-treated cells. In fact, PGC-1α mRNA expression in the differentiated control cells was at least ten-fold greater than in the CA-treated cells.

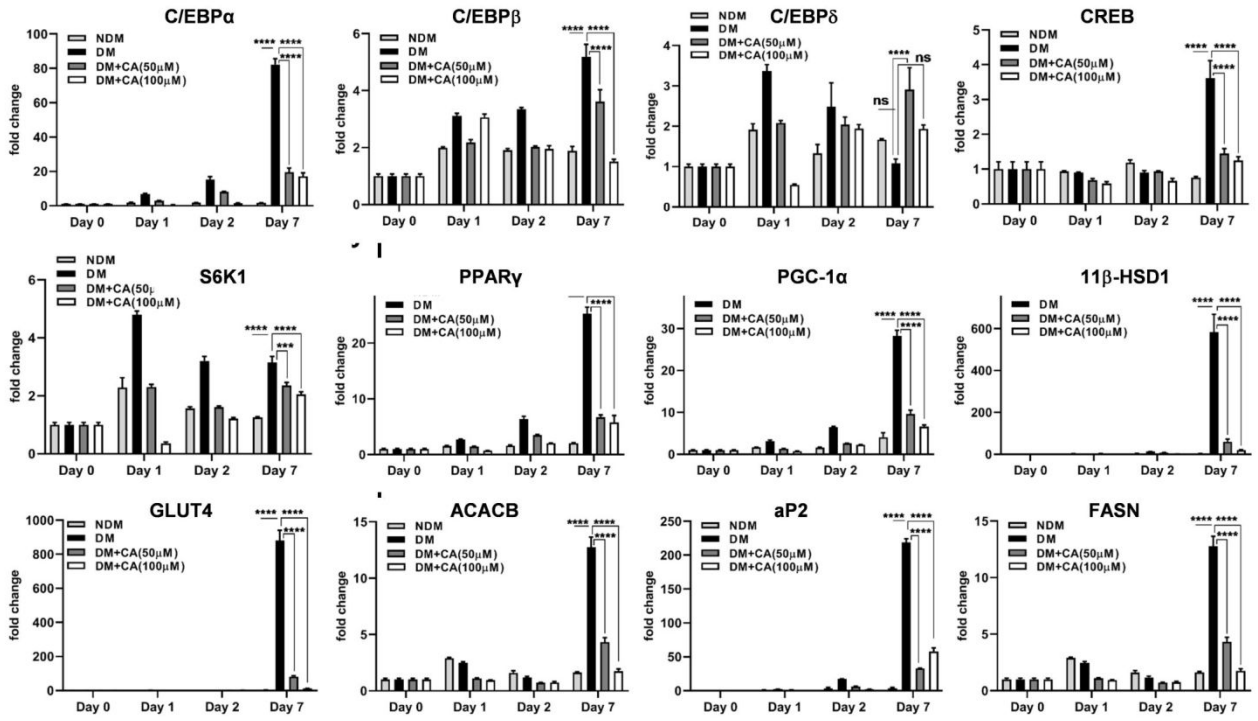

Figure 8. Differential gene expression during the 3T3-L1 adipogenesis assay on days 0, 1, 2 and 7. The steady-state mRNA levels were analyzed according to the ΔCt method using β-actin, PP1A and PP1B as housekeeping genes with their calculated geometric mean for each sample as standardized Ct [i.e. 2(Ct,HK–Ct,target)−1 (Pfaffl et al., 2004)].[35] Specific primers sets of each gene were used to amplify single products (Table S5, Supporting Information). The values represent the means ± SEM, n = 3. Significant differences between the groups by using ANOVA's one-way followed by post-test and are indicated by asterisks; ****$p < 0.0001$; ***$p < 0.001$; **$p < 0.01$; *$p<0.05$; ns, not significant ($p>0.05$).

Expression of 11β-HSD1 mRNA was also reduced in the CA-treated cells when compared with the differentiated control cells. Furthermore, a comparable pattern was observed for the mRNA expression of Glucose Transporter 4 (Glut4) and Acetyl-CoA carboxylase beta (ACACB), both genes involve in regulation of metabolism. Finally, the mRNA expression of terminal marker genes of adipogenesis, Fatty Acid Binding Protein 4 (FABP4, also known as AP2), and Fatty Acid Synthase (FASN) were evaluated. The mRNA expression levels in the CA-treated cells were at least 10-fold lower than in the differentiated control cells. The combined data suggests that CA-treated cells are prevented from committing to the differentiation program during induction, and the lipid formation program was suppressed at the late stage of adipogenesis.

To confirm that gene expression changes correlated with protein expression level, western blot (WB) analyses at days 3 and 7 were conducted in 3T3-L1 cell model. Indeed, congruency was observed between RNA and protein expression, particularly for 11β-HSD1, PPARγ, and PGC-1α (Figure S13, Supporting Information). No substantial 11β-HSD1, PPARγ, and PGC-1α expression differences were detected between non-differentiating medium (NDM) treated control cells and differentiating medium (DM) treated control cells at day 3 (Figure 9). However, significant increase of these protein expression levels was recorded by day 7 in the DM treated cells. In the CA-treated cells, expression levels remain comparable to those in NDM cells, suggesting that CA also effectively suppress the protein expression of these genes, particularly PPARγ at the late stage of adipogenesis. Thus, CA could prevent adipocyte hypertrophy via PPARγ suppression as described by Iwabu *et. al*.[38] In addition, total GR expression remained largely unchanged for day 3 and 7 under the different experimental conditions (Figure S13, Supporting Information).

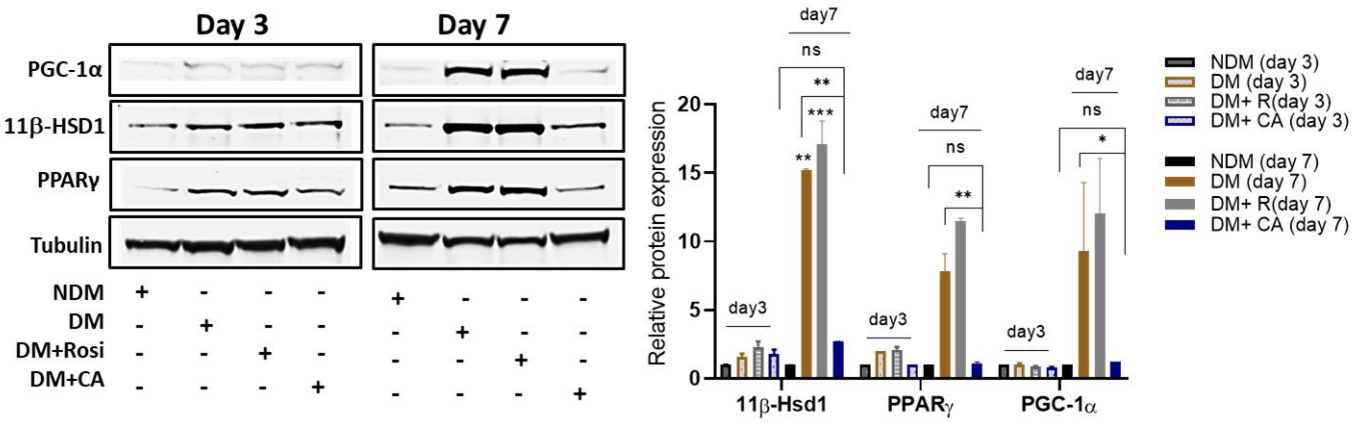

Figure 9. CA-treated 3T3-L1 differentiating cells showed down-regulation of PGC-1α, 11β-HSD1, and PPARγ expression by day 7. No significant change was detected for day 3. Representative Western blot (30 μg of total protein and tubulin was used as the loading control) and quantification of day 3 and day 7 samples. NDM–treated control cells, DM–treated control cells, DM-treated with Rosiglitazone (Rosi) and DM-treated with CA (50 μM)-treated cells. The values represent the means ± SEM, n = 3. Significant differences between groups are indicated by asterisks; ***$p < 0.0001$; **$p < 0.002$; *$p < 0.01$; ns, not significant ($p>0.05$).

The significant reduction of PGC-1α expression at the RNA and protein level for the CA treated cells when compared to DM control cells led us to interrogate whether mitochondrial density was affected by using live-cell imaging with a mitochondrial tracker (magenta) for 3T3-L1 cells during adipogenesis. PGC-1α is a regulator of energy metabolism and promotes fatty acid oxidation, which stimulate mitochondrial biogenesis to provide the required energy for lipid synthesis and storage.[29,38] The mean intensity of mitochondrial tracker (magenta) staining for each treatment group along with nuclear Hoechst stain (blue) was captured with a confocal imaging system and it is shown in Figure 10. The resulting findings clearly illustrated higher mitochondrial mass for the differentiated cells (Figure 10B), while both the NDM (Figure 10A) and the CA-treated cells (Figure 10C) displayed less mitochondrial

mass as relative quantified (Figure 10D). The images confirmed that PGC-1α expression correlates with mitochondrial mass, and that CA inhibits the required signaling for lipid deposit formation.

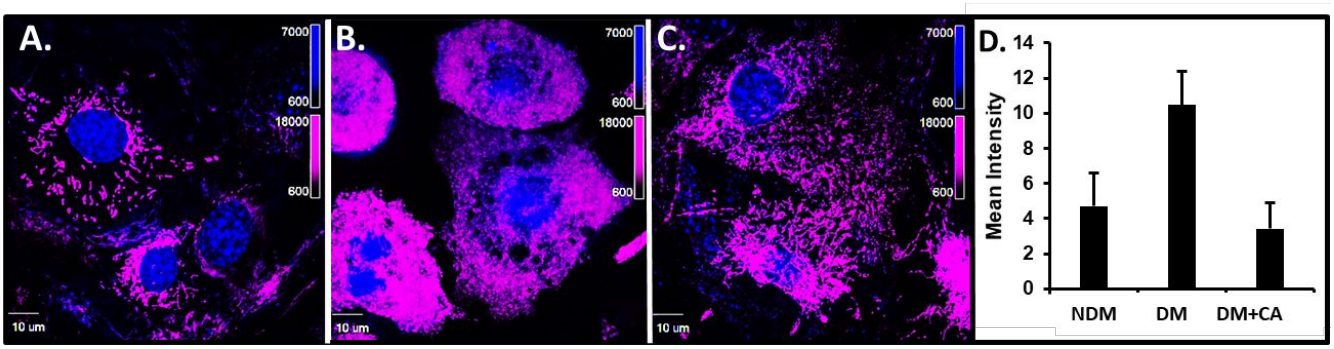

Figure 10. Live-cell images of 3T3-L1 adipogenesis assay stained with mitochondrial tracker (magenta) and nuclear stain (blue). (A) NDM control cells. (B) DM–treated control cells. (C) DM–treated CA (50 μM). (D) Mean intensity of mitochondrial tracker. Imaged on a Marianas spinning disk confocal imaging system at 63× magnification.

Although no detection of cytotoxicity upon CA treatment at the effective concentrations, protein synthesis inhibition could affect cellular commitment without causing cell death. Protein synthesis and cellular degradation are closely regulated processes that enable cells to adapt during fluctuating environmental conditions. Thus, using a global protein synthesis assay, CA was evaluated for alterations in intracellular protein homeostasis in a fibroblast cell model (Figure 11). The method is based on an alkyne containing o-propargyl-puromycin probe, which stops translation by covalently binding with nascent polypeptide chains. Then, the truncated polypeptides are rapidly turned over by the proteasome and can be detected based on the subsequent click reaction with a fluorescent azide[39] (red), and the counter DNA stain picogreen (green) for overall evaluation of the cell. The protein synthesis inhibitor, cycloheximide was used as the positive control. No significant changes were observed for CA treated

cells as compared to DMSO control. Several time points were evaluated, but no protein synthesis inhibition was observed over time (data not shown).

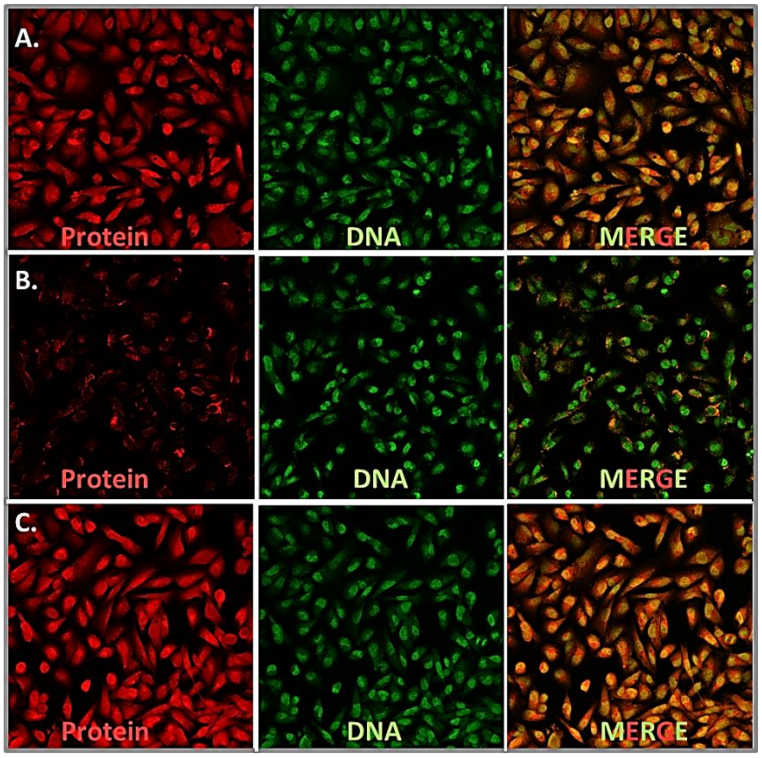

Figure 11. Evaluation of protein synthesis by using a global protein synthesis assay. (A) Vehicle (DMSO). (B) Cycloheximide (20 nM, positive control). (C) CA (50 μM). Nascent protein (red), DNA (green) and merged representative images at 20× magnification with a Nikon C2 scanning confocal microscope for 3 independent experiments.

To investigate the possibility that CA interacts directly with PPARγ and GR, both of which directly influence the differentiation process, supporting assays were conducted. First the potential of CA to bind or directly affect the GR activation was evaluated. A transiently transfected mammalian cellular model using a GR response element–driven luciferase DNA construct was used.[40] Cell were treated with CA or vehicle in the presence of dexamethasone and CA treatment did not inhibit GR activation (Figure 12), suggesting that CA does not directly bind to GR. This data indicates that CA does not affect GR

activation in non-GR dependent cellular models, and the observed adipogenesis inhibition is primarily due to selective inhibition of 11β-HSD1.

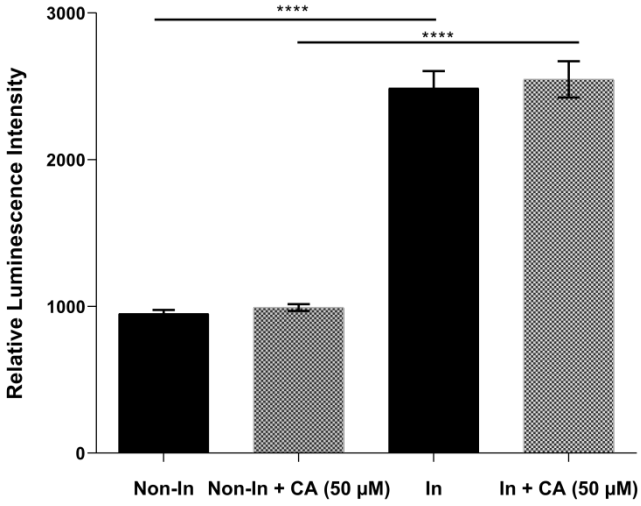

Figure 12. Human GR reporter assay showed CA did not affect GR activation. Glucocorticoid receptor (GR) functional activation. Transiently GR-transfected cells were induced (In) by treatment with 100 nM dexamethasone. Cells were treated with colletoic acid (CA) 1 h prior to GR induction. Control cells were non-induced (Non-In). The values represent the means ± SEM, n = 3. Significant differences between groups are indicated by asterisks; ****$p < 0.0001$.

Finally, the cellular PPARγ reporter assay kit[41] was used to evaluate whether CA affects this important transcriptional factor. Previous studies of transcriptional antagonists of PPARγ have demonstrated adipogenesis inhibition in 3T3-L1 cells.[27] The potent irreversible PPARγ antagonist GW9662 was used as a positive control (Figure 13). CA showed no quantifiable PPARγ antagonistic activity, indicating CA does not directly interact with PPARγ.

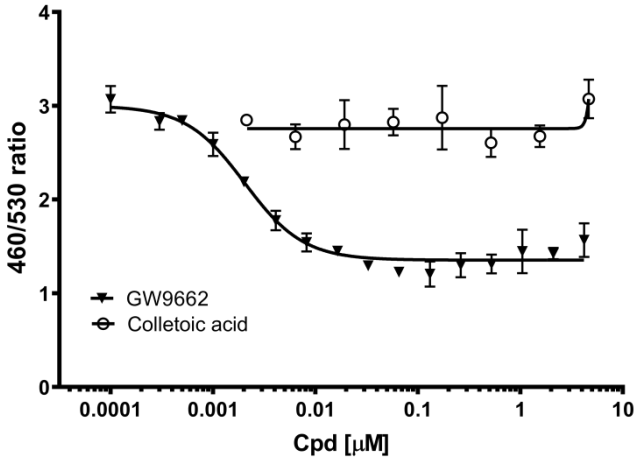

Figure 13. Human PPARγ reporter antagonist assay. Transcriptional response of colletoic acid after stimulation by rosiglitazone (20 nM) during PPARγ reporter assay. Irreversible PPARγ antagonist GW9662 was used as a control (EC_{50} = 2 nM). Colletoic acid did not show antagonistic effect in this PPARγ reporter assay at the tested concentrations.

Physicochemical Properties and its Analogues. Lipophilic efficiency (LipE), also known as lipophilic ligand efficiency, is a metric that normalizes lipophilicity relative to potency, aiding in prioritizing lead compounds. Thus, LipE and in vitro ADME properties were evaluated for CA and its active analogues (**9**, **18**-**20**, Table S1, Supporting Information). Interestingly, CA displayed the best LipE (3.5) while compound **20** (3.3) was comparable to CA. Overall the solubility properties of compound **19** and **20** were acceptable and similar to CA, but further improvement would be necessary for in vivo efforts. Metabolic stability was evaluated by microsomal assay using mouse (m) and human (hs) liver microsomes: CA (m t1/2=1.33 h; hs t1/2=1.18 h), compound **18** (m t1/2=0.3 h; hs t1/2=1.29 h), compound **19** (m t1/2=0.27 h; hs t1/2=0.93 h) and compound **20** (m t1/2=0.13 h; hs t1/2=0.3 h) showed rapid clearance in mice, while they were more stable in human microsomes. Conversely, compound **9** (m t1/2=2.23 h; hs t1/2=6.8 h) showed the highest metabolic stability, indicating that the C-

9 hydroxyl group might be responsible for the observed clearance. However, human plasma stability assay was remarkably high for all the tested compounds, CA, **9**, **18-20** (t1/2> 48 h). A similar trend was recorded in mouse plasma for this set of compounds except for CA, which showed poor mouse plasma stability. Simulated gastric fluid stability assay was not optimal for CA (<2 h), but it was promising for compounds **9**, **18-20** (> 6 h). Thus, preliminary PK/PD studies of CA (Table S2, Supporting Information) were conducted to test its in vivo potential. However, in vivo systemic unfavorable plasma clearance was observed with a volume of distribution at steady-state (V_{SS}) was close to the predicted (Obs V_{SS} 0.247 ± 0.169 L/kg, ACD Pred 0.33 L/kg), which indicates that further development of CA is required for in vivo investigations. However, the combined studies indicate there is ample opportunities for improvement of the physicochemical properties of the CA scaffold using bioisostere strategies (C-9 hydroxyl group replacement), and/or prodrug formulation/liposome delivery systems. This study demonstrated opportunity for CA's medicinal chemistry optimization, suggesting its potenital utility in animal models.

CONCLUSIONS

In summary, we describe the design, synthesis, and cellular evaluation of CA analogues as selective inhibitor of 11β-HSD1, providing mechanistic insights on the mode of action of CA in adipocyte biology. CA shows no cytotoxicity at the tested concentration, therefore it can serve as a selective chemical probe to enable an in-depth dissection of the role of GC signaling during adipocyte differentiation via pharmacological inhibition of 11β-HSD1. A comprehensive SAR analysis of CA revealed a strong correlation between the functional groups at C-1, C-4, and C-9. We have solved the first X-ray crystal structure of the 11β-HSD1-CA complex, highlighting the sterically demanding all-carbon quaternary spirocycle, which leads to a tight binding complex via interactions of Ser170/Tyr183 with the carboxyl group at C-1 of CA, and interactions of the hydrophobic residues of the catalytic site

(Thr124, Leu126, and Val180) with the alkyl substituent at C-4 of CA, thus providing ligand stabilization, which was congruent with our SAR studies. The pseudo-transition state of such binding mode provides rational for the high selectivity of CA to 11β-HSD1. The combined efforts led to a superior CA analogue, namely compound **20**, which was developed by introducing a bulky cyclohexyl group at C-4 and displayed a three-fold increase in potency than CA. CA did not inhibit *de novo* protein synthesis, and under preadipocyte differentiating conditions reduced mitochondria biogenesis. We demonstrate that CA inhibits adipocyte differentiation in both murine and human cellular models at the early stage of adipogenesis. No cellular toxicity was observed during CA treatment, thus the decrease of PPARγ, and Glut4 during adipogenesis can be solely attributed to 11β-HSD1 inhibition. The demonstrated synthetic manipulations of the CA core render it now feasible for the development of fluorescent/radio probe for live-cell[42] or in vivo imaging studies.[5c] Additional in-depth cellular studies aimed at evaluating CA analogues in combination with other therapies are warranted, as attenuating adipogenesis by selectively inhibiting 11β-HSD1 may represent an alternative approach to prevent adipocyte dysfunction in MetS related disorders.

EXPERIMENTAL SECTION

General Chemistry. All reactions were carried out under argon atmosphere, and anhydrous conditions, unless noted otherwise. Dry tetrahydrofuran (THF), toluene, diethyl ether (Et_2O), ethyl acetate (EtOAc) and methylene chloride (CH_2Cl_2) were obtained by passing commercially available pre-dried, oxygen-free formulations through activated alumina columns. Acetonitrile (CH_3CN), dimethyl sulfoxide (DMSO), and isopropanol were purchased in anhydrous form and used without further purification. Yields refer to chromatographically and spectroscopically (^1H NMR) homogeneous materials, unless otherwise stated. Reagents of the highest available quality were purchased and used without further purification, unless otherwise stated. Reactions were magnetically stirred and monitored

by performing thin-layer chromatography (TLC) on 0.25 mm silica gel 60 F_{254} TLC plates (Merck) using UV light for visualization and an ethanolic solution of anisaldehyde and heat as developing agents. Reaction progress was also monitored by using Agilent 1100 series LCMS and a low-resonance electrospray model (ESI) with UV detection at 254 nm. Title compounds were purified by flash column chromatography via E. Merck silica gel (60, particle size 0.040–0.063mm) or Biotage Isolera Four with normal-phase silica gel. ^{1}H and ^{13}C nuclear magnetic resonance (NMR) spectra were recorded on a Bruker NMR spectrometer (AV-400 or DRX-500 MHz) calibrated with residual non-deuterated solvent ($CDCl_3$: δ_H =7.26 ppm, δ_D =77.16 ppm; acetone-d_6: δ_H =2.05 ppm, δ_C =29.84ppm; CD_3CN: δ_H =1.94ppm, δ_C =1.32ppm; CD_3OD: δ_H =3.31ppm, δ_C =49.00 ppm; DMSO-d_6: δ_H =2.50ppm, δ_C =39.5ppm) used as an internal reference. The following abbreviations were used to designate the multiplicities: s=singlet, d=doublet, t=triplet, q=quartet, quin=quintet, hept=heptet, m=multiplet, and br=broad. Infrared (IR) spectra were recorded on a Perkin-Elmer100 FT-IR spectrometer. High-resolution mass spectra (HRMS) were recorded on an Agilent ESI-time of flight (ESI-TOF) mass spectrometer using matrix-assisted laser desorption ionization or ESI or on a Waters Xevo G2 Q-ToF mass spectrometer. Compounds were analyzed by using electrospray ionization in positive-ion mode. The purity of final compounds was >95% based on analytical HPLC and NMR analysis. Procedures for all intermediates can be found in the Supporting Information.

(-)-Colletoic Acid (*ent*-**1**). To a solution of compound **21x** (20.0 mg, 0.07 mmol) in THF (1.0 mL) and methanol (0.20 mL) at 0 °C, aqueous sodium hydroxide (0.10 M, 0.10 mL) was added. The reaction mixture was stirred at 0 °C for 1 h, diluted with brine (3.0 mL) and extracted with EtOAc (3 × 1.0 mL). The aqueous phase was carefully acidified at 0 °C (pH~3.0) and underwent extraction with EtOAc (3 × 1.0 mL). The combined organic phase was dried over anhydrous $MgSO_4$, concentrated under reduced pressure, and purified by silica gel column chromatography (EtOAc: Hexane, 10-50%, v/v) to afford (-)-

colletoic acid, *ent*-**1** (15.0 mg, 0.06 mmol, 86% yield). $[\alpha]_D^{22}$ = -16.80° (c 0.10, MeOH); ^{1}H NMR (599 MHz, Chloroform-*d*) δ 5.47 (s, 1H), 4.04 (s, 1H), 2.82 (dd, *J* = 10.3, 5.8 Hz, 1H), 2.24 (dd, *J* = 14.6, 6.0 Hz, 1H), 2.21 – 2.14 (m, 1H), 2.12 – 2.05 (m, 1H), 2.0 – 1.0 (m, 10H), 0.96 (d, *J* = 6.7 Hz, 3H), 0.88 (d, *J* = 6.7 Hz, 3H). ^{13}C NMR (151 MHz, $CDCl_3$) δ 181.55, 134.42, 124.42, 68.19, 58.05, 53.08, 47.20, 44.10, 27.81, 27.01, 26.93, 25.69, 24.92, 21.19, 20.21; HRMS (EI) calcd for $C_{15}H_{24}O_3Na$ ($M + Na^+$): 275.1623, found: 275.1633.

*Synthesis of Compounds **18*** and ***19***. To a solution of compound **20o** (0.14 g, 0.35 mmol) in acetic acid (1.20 mL), platinum (IV) oxide (Adam's catalyst, 8.0 mg) was added. The reaction was stirred under hydrogen atmosphere (1 atm) for 5 h at room temperature (RT). The reaction mixture was filtered through a short celite plug, and water (3.0 mL) was added to the filtrate and extracted with EtOAc (3 × 1.0 mL). The combined organic layer was dried over anhydrous $MgSO_4$ and concentrated under reduced pressure to afford the reduced product, which was directly used for the next step without further purification. A solution of the above reduced product in THF (10.0 mL) was cooled to 0 °C, followed by addition of diisobutyl aluminum hydride (DIBAL-H, 1.0 M in THF, 0.40 mL, 0.40 mmol) under nitrogen atmosphere, the reaction mixture was stirred at the same temperature for additional 30 minutes before quenched by the careful addition of aqueous $Na_2S_2O_3$ (10.0 mL). The suspension was then diluted with EtOAc (10.0 mL) and filtered through a short column of celite which was rinsed with additional EtOAc (2 x 5.0 mL). The organic phase was separated, and aqueous layer was extracted twice with EtOAc (2 x 5.0 mL). The combined organic phase was dried over anhydrous $MgSO_4$ and concentrated under vacuo to provide the dried crude alcohol product compound **22e**, which was subjected to the next steps without further purification. Compound **22e** (0.30 mmol) was dissolved in anhydrous CH_2Cl_2 (5.0 mL) and pyridine (1.0 mL, excess), followed by addition of acetic anhydride (0.05 mL, 0.40 mmol) and 4-dimethylaminopyridine (2.0 mg, 0.013 mmol). The reaction mixture was

stirred for 16 h at RT and quenched with aqueous solution sodium bicarbonate (10.0 mL), followed by extraction with CH_2Cl_2 (3 × 10.0 mL); the combined organic phase was dried over anhydrous $MgSO_4$, concentrated under reduced pressure to afford the dried crude product, which was used in the next step without further purification. A solution of the resultant product **22f** in anhydrous CH_2Cl_2 (5.0 mL) and pyridine (5.0 mL, excess) was cooled to 0 °C, followed by addition of thionyl chloride (30.0 μL, 0.40 mmol) and stirred for 1 h at this temperature. The reaction mixture was then quenched with aqueous sodium bicarbonate solution (15.0 mL), extracted with CH_2Cl_2 (3 × 10.0 mL). The combined organic phase was dried over anhydrous $MgSO_4$, concentrated under reduced pressure to afford the crude product **22g** which was used for the next step without further purification. The above crude product residue **22g** was dissolved in THF (5.0 mL), followed by addition of TBAF (1.0 M in THF, 0.80 mL, 0.80 mmol), the reaction mixture was stirred at 25 °C for 1 h, followed by quenching with brine (15.0 mL) and extraction with EtOAc (3 × 10.0 mL), the combined organic phase was dried over anhydrous $MgSO_4$, concentrated under reduced pressure, and the residue was purified by silica gel column chromatography (EtOAc: Hexane, 10-30%, v/v) to afford compound **22h** (67.0 mg, 0.21 mmol, 70% overall yield, 3 steps from compound **22e**). To a solution of oxalyl chloride (0.09 mL, 1.0 mmol) in dry CH_2Cl_2 (5.0 mL) was added dimethyl sulfoxide (0.11 mL, 1.60 mmol) at was added −78 °C in an argon atmosphere and stirred for 5 min. Then compound **22h** (65.0 mg, 0.20 mmol) in CH_2Cl_2 (5.0 mL) was added to the above reaction mixture at −78 °C and stirred for 1 h at the same temperature. The reaction mixture was quenched with anhydrous triethylamine (0.32 mL, 2.30 mmol) and allowed to slowly warm up to 0 °C in 1 h. An aqueous ammonium chloride solution (10.0 mL) was added to the reaction mixture, followed by extraction with CH_2Cl_2 (3 × 10.0 mL), the combined organic phase was dried over anhydrous $MgSO_4$ and concentrated under reduced pressure to afford the crude aldehyde, which was used for the next step without further purification. To a solution of the crude aldehyde in THF (3.0 mL)

and water (3.0 mL), was added 2-methyl-2-butene (0.20 mL, excess) and sodium dihydrogen phosphate (0.07 g, 0.60 mmol) at 0 °C, followed by addition of sodium chlorite (32.0 mg, 0.34 mmol), and stirred for additional 1 h at the same temperature. The reaction mixture was quenched with brine (10.0 mL), followed by extraction with EtOAc (3 × 10.0 mL), the combined organic phase was dried over anhydrous $MgSO_4$, concentrated under reduced pressure and purified by silica gel column chromatography (EtOAc: Hexane, 10-50%, v/v) to afford carboxylic acid compound **22hh**, which was subjected to the next steps without further purification. To a solution of the above carboxylic compound 22hh in THF (1.0 mL) and methanol (0.20 mL) at 0 °C, aqueous sodium hydroxide (0.10 M, 0.10 mL) was added. The reaction mixture was stirred at 0 °C for additional 1 h, diluted with brine (3.0 mL) and extracted with EtOAc (3 × 1.0 mL). The aqueous phase was carefully acidified at 0 °C (PH~3.0) and extracted with EtOAc (3 × 3.0 mL). The combined organic phase was dried over anhydrous $MgSO_4$, concentrated under reduced pressure, and purified by silica gel column chromatography (EtOAc: Hexane, 10-50%, v/v) to afford compound **18** (35.0 mg, 0.12 mmol, 60% overall yield, 3 steps from compound **22h**) and compound **19** (13.7 mg, 0.05 mmol, 25% overall yield, 3 steps from compound **22h**). (1S,4S,5S,10R)-4-Cyclohexyl-10-hydroxy-8-methylspiro[4.5]dec-7-ene-1-carboxylic acid (**18**): ^{1}H NMR (500 MHz, Chloroform-d) δ 5.25 (s, 1H), 3.93 (dd, J = 7.8, 5.9 Hz, 1H), 3.35 (q, J = 7.2 Hz, 1H), 2.96 – 2.86 (m, 1H), 2.50 – 0.70 (m, 22H). ^{13}C NMR (126 MHz, CD3CN) δ 181.06, 131.45, 120.64, 71.65, 52.99, 50.06, 47.28, 37.55, 37.12, 34.86, 31.79, 28.32, 27.07, 27.05, 26.75, 26.54, 26.42, 22.63. HRMS (EI) calcd for $C_{18}H_{29}O_3$ (M + H+), 293.2117; found, 293.2124.

(1S,4S,5S)-4-Cyclohexyl-8-methylspiro[4.5]deca-6,8-diene-1-carboxylic acid (**19**): ^{1}H NMR (500 MHz, Chloroform-d) δ 5.72 (dd, J = 9.6, 1.6 Hz, 1H), 5.43 (d, J = 9.6 Hz, 1H), 5.23 (s, 1H), 2.75 – 1.62 (m, 22H). ^{13}C NMR (126 MHz, CDCl3) δ 179.58, 135.07, 130.21, 126.49, 120.15, 57.90, 53.19, 49.36,

39.55, 32.71, 32.53, 27.31, 26.56, 26.52, 26.31, 23.91, 23.59, 20.91. HRMS (EI) calcd for $C_{18}H_{27}O_2$ (M + H^+), 275.2011; found, 275.2013.

*Compound **20***. To a solution of compound **20x** (110.0 mg, 0.33 mmol) in THF (1.0 mL) and methanol (0.20 mL) at 0 °C, aqueous sodium hydroxide (0.10 M, 0.10 mL) was added. The reaction mixture was stirred at 0 °C for additional 1 h, diluted with brine (3.0 mL) and extracted with EtOAc (3 × 1.0 mL). The aqueous phase was carefully acidified at 0 °C (PH~3.0) and extracted with EtOAc (3 × 3.0 mL). The combined organic phase was dried over anhydrous $MgSO_4$, concentrated under reduced pressure, and purified by silica gel column chromatography (EtOAc: Hexane, 10-50%, v/v) to afford (1S,4S,5S,9S)-4-cyclohexyl-9-hydroxy-8-methylspiro[4.5]dec-7-ene-1-carboxylic acid (**20**) (33.0 mg, 0.11 mmol, 33% yield from compound **20x**). Note compound **20** will undergo spontaneous lactonization in slightly acidic $CDCl_3$ NMR solvent, therefore NMR is reported in acetonitrile-d_3. ^{1}H NMR (500 MHz, Acetonitrile-d_3) δ 5.45 (s, 1H), 4.11 (d, J = 4.8 Hz, 1H), 2.82 (dd, J = 10.4, 4.6 Hz, 1H), 2.30-0.80 (m, 23H); ^{13}C NMR (126 MHz, CD_3CN) δ 178.06, 134.53, 125.59, 68.67, 60.92, 58.74, 54.32, 46.97, 44.34, 37.85, 36.31, 32.35, 28.78, 27.97, 27.84, 27.40, 27.18, 26.38, 20.49, 14.47. HRMS (EI) calcd for $C_{18}H_{29}O_3$ (M + H^+), 293.2117; found, 293.2114.

Biochemical Assay of 11β-HSD1. The sequence encoding 11β-HSD1 was modified to include a single substitution (C272S) and an N-terminal tag (MKHQHQHQHQHQHQQPL) to facilitate purification as previously reported.[22] The modified sequence was inserted into the PJexpress404:97590 expression vector by DNA 2.0, and the plasmid was used to transform competent E. coli BL21[DE3] cells. Cells were induced with 1 mM isopropyl-β-D-thiogalactopyranoside and treated with 1 mM corticosterone for 12 h at 18 °C. Then, cells were lysed by sonication in 50 mM Tris (pH 8), 500 mM NaCl, 5 mM imidazole, 4 mM CHAPS, lysozyme, and protease inhibitor cocktail (Roche 11-836-170-001). The protein was purified by a two-step protocol a) elution from a Ni2+-affinity chromatography

column using a gradient of 50-500 mM imidazole, and b) size-exclusion chromatography on a 16/60 Sephacryl 200 column (250 mM NaCl, 25 mM Tris pH 7.9, and 4 mM CHAPS). High-resolution mass spectroscopy and western blotting with 11β-HSD1 antibody (abcam ab39364) confirmed the expected MW. Next the inhibition constant (Ki) of experimental compounds was measured as a function of cortisol concentration, and IC_{50} values were calculated by the Cheng-Prusoff equation: IC_{50} = Ki x(1+[s]/Km). The assay required the incubation of a solution of 1.5 μM 11β-HSD1 with varying amounts of cortisol (0-200 μM) using assay buffer (50 mM TRIS pH 7.5, 150 mM NaCl, 0.5 mM EDTA, 0.01% Brij35, and 200 μM NADP+) in Greiner 384-well black plates and incubated at 37 °C. After NADPH formation, the change in fluorescence intensity was measured in a Pherastar LS plate reader with a wavelength setting of 360 nm for excitation and 460 nm for emission for 1 h. Data were fit to a competitive inhibition model by using GraphPad Prism software, Version 7.02. Representative experimental results are shown in Figure S1 (Supporting Information).

Biochemical Assay of 11β-HSD2. Reductase activity of 11β-HSD2 was measured via Cisbio's HTRF Cortisol assay kit (Cat. No. 62CRTPEB; Cisbio, USA) according to the manufacturer's protocol. Enriched 11β-HSD2 cell lysates were prepared from an HEK293 cellular model constitutively expressing 11β-HSD2 (GeneCopoeia plasmid, human HSD11B2 Catalog No.: EX-C0760-M51). A cell pellet (50×10^6) was resuspended in 1 mL TS2 buffer, sonicated, and centrifuged at 17000 g for 5 min at 4 °C. The soluble fraction was collected, and the protein concentration (6-7 mg/mL) was determined by using the BCA protein assay kit (Pierce, USA). The 11β-HSD2 activity assay was conducted in TS2 buffer containing 2.66 μM Cortisone, 3.33 μM NAD+, and 10% (v/v) vehicle (dimethyl sulfoxide [DMSO] or compound) in a total volume of 10 μL. The reaction mixture was incubated for 2 h at 37 °C, followed by quenching with 1 μL of 10 mM carbenoxolone, 5 μL d2-labeled cortisol, and 5 μL cryptate-labeled anti-cortisol MAb. Then, the mixture was incubated for 2 h at RT, and fluorescence was

recorded by using a BMG Pherastar plate reader equipped with an excitation filter of 337 nm, a first-emission filter of 665 nm, and a second-emission filter of 620 nm in optic HTRF module. Data analysis was conducted according to the manufacturer's instructions (Cisbio, USA) and is shown in Figure S2 (Supporting Information).

X-ray Studies. Crystallization, structure determination, and model quality of 11β-HSD1 with colletoic acid: The 11β-HSD1 protein construct described above was used for crystallization analysis. The 11β-HSD1 was crystallized by hanging-drop vapor diffusion at 18 °C. The 4-μL drop contained 2 μL of protein (25 mM Tris, pH 8.0, 250 mM NaCl, 4 mM CHAPS, 10 mg/mL protein), and 2 μL of well solution (100 mM MES, pH 6.5, 20% PEG 4000). Previous attempts to soak CA cracked the crystals. Therefore, glutaraldehyde was added to the well solution (0.1 % final concentration) to induce cross-linking of the protein crystal 2 h before the addition of CA. The crystal was soaked for 20 h with 1 mM CA and cryopreserved in 20% (v/v) ethylene glycol/ 80% (v/v) well solution. Native data (1.0 Å) were collected at SER-CAT 22ID to 2.6 Å. The 2.55-Å crystal structure of 11β-HSD1 (3D5Q), with NADP(H) and inhibitor molecules removed, served as the Phaser[43] molecular replacement model. The crystals belong to space group $P2_1$, with 4 11β-HSD1 protomers in the asymmetric unit arranged as a tetramer (dimers A/B and C/D). Cofactor NADP(H) and CA were observed in all protomer active sites in the initial maps. However, only NADP(H) was modeled initially. After rigid body refinement and simulated annealing, CA was added to the model. Subsequent refinement included SA, minimization, and B factor refinement. Non-crystallographic symmetry restraints were used until the later stages of refinement. Model building was performed by using *Coot* map-building tools.[44] Initial structure refinement, including SA was performed with Phenix[43]; later stages of refinement were performed with Refmac, and 5% of the data were sequestered to calculate R_{free}. The final model is of good quality, as shown in Table S1 (Supporting Information). Because of insufficient electron density, neither *N*-

terminal His-tag residues for protomers nor *N*- and C-terminal residues A24-33, A282-292, B24-25, B283-292, C24-25, C281-292, D24-27, or D283-292 were modeled. Poor electron density also prohibited incorporation of residues 66-70 from chain D and the 'variable loop' for chains A, C, and D. Side chains with unclear density were modeled as alanine amino acids. Chain A has the best quality electron density for CA and surrounding protein-contacting residues and is the chain used to describe the structure, unless otherwise noted. Chain D has the poorest quality electron density overall, and the conformation of CA modeled into the weaker electron density was based on the conformation observed in pockets A, B, and C after SA. Ramachandran statistics show that 91.5%, 7.9%, and 0.6% of the residues are in the respective preferred, allowed, and disallowed regions. The final structure statistics were calculated by using MolProbity.[44] Structural figures were generated by using PyMOL.[45] The electron density rendering map is shown in Figure S3 and a close-up view of the CA bound in the catalytic site with cofactor $NADP^+$ is shown in Figure S4 (Supporting Information).

Cell Culture. All cellular models were incubated at 37 °C and maintained in an atmosphere containing 5% CO_2 and in accordance with sterile cell culture practices. Cell lines were tested for Mycoplasma (MycoAlert™, cat# LT07-318, Lonza) every 2 weeks by using the manufacturer's conditions. Cell lines were purchased from American Type Culture Collection (ATCC®). HEPG2 (ATCC, HB-8065, human liver carcinoma), BJ (ATCC, CRL-2522, normal human foreskin fibroblast), HEK-293 (ATCC, CRL-1573, transformed human embryonic kidney cell line); and murine models 3T3-L1 (ATCC, CL-173), J774.1 (ATCC# TIB-67) and MEF (ATCC# CRL-2907) cells. Cells were grown in medium (DMEM, EMEM, IMDM or Basal medium) containing 10% fetal bovine serum (FBS, Hyclone), 2 mmol L-glutamine (GlutaMAX™), and 1% penicillin/streptomycin (for murine models) or gentamicin sulfate (50 μg/mL for human preadipocytes) to densities recommended by ATCC. The 3T3-L1 murine fibroblast is an accepted cellular adipogenesis model since it competently undergoes

adipogenesis after treatment with induction medium and experiments were conducted with passages 1-16. For The human subcutaneous preadipocytes (Poietics™, PT-5020, Lonza) and visceral preadipocytes (PT-5005, Lonza) were cultured according to the manufacturer's instructions up to passage 3 (Figure S12, Supporting Information).

Cytotoxicity Assay. Cytotoxicity was assayed by using the CellTiter-Glo (CTG) Luminescent Cell Viability Assay kit (G7570, Promega) according to the manufacturer's instructions. Luminescence was measured by using a plate reader (Envision, Perkin Elmer). Cells were then added to 384-well white flat-bottomed plates (400-1250 cells per well in 30 μL total volume) or 96-well flat bottom plates (2500-5000 cells per well in 100 μL total volume). The plates were incubated at 37 °C in a 5% CO_2 atmosphere for 24 hours (h). Stock solutions of test compounds (10 mmol in DMSO) in nine 3-fold serial dilutions were dispensed via pintool. The final concentration of DMSO was 0.3% (v/v) in each well. The plates were incubated for 72 h at 37 °C in a 5 % CO_2 atmosphere and then quenched with CTG reagent at RT. The positive controls were staurosporine (25 μM), gambogic acid (10 μM), and N^1-(5-fluoro-2-methoxybenzyl)-N^3-(7-(3-(trifluoromethyl)benzyl)quinolin-4-yl)propane-1,3-diamine (1 μM).

Annexin V-FITC Apoptosis and Cell Cycle. The samples were probed with Annexin V-FITC (Roche/Boehringer Mannheim) according to the manufacturer's instructions. Briefly, 3T3-L1 cells were plated (1.00×10^6 cells/plate) and incubated for 12 h at 37 °C. Cells were treated with CA or controls for 24 h under the specified conditions, then stained with AnnexinV-FITC and PI. Cells were fixed with cold methanol, treated with RNase, and stained with PI solution (50 μg/mL). The Annexin profiles and cell-cycle distribution were determined with FACSCalibur analyzer (BD Biosciences, Franklin Lakes, NJ, USA) and analyzed with Cell-Quest software (Aliso Viejo, CA, USA) and ModFit-software (Verity Software House, ME, USA).

Preadipocyte Differentiation Assay. Non-differentiated preadipocytes, 3T3-L1 cellular model was cultured in DMEM (ATCC, 30-2002) supplemented with newborn calf serum (BioWorld CAT#30611076-1), 100 U/mL penicillin and 100 mg/mL streptomycin. For adipogenesis experiments, cells were seeded in 9.61-cm^2 6-well dishes at a density of 2.5×10^5 cells/dish. Plates were coated with 0.1% gelatin. After 24 h at near 100 % culture confluency (day 0), the medium was changed to induction medium [DMEM (high glucose) containing 10% FBS, 100 U/mL penicillin, 100 mg/mL streptomycin, 0.5 mM isobutyl-1-methylxanthine (IBMX; I5879, Sigma-Aldrich), 0.25 μM DHC (D3224, Biomol), 0. 250 μM cortisone (C2755, Sigma-Aldrich) or 0.10 μM dexamethasone (D2915, Sigma-Aldrich), 5 μg/mL insulin (I9278, Sigma-Aldrich)]. Positive controls included DMSO and 2 μM rosiglitazone Cayman Chemicals (Ann Arbor, MI). The compounds of interest were added during induction. Non-differentiating 3T3-L1 preadipocytes (negative control) were maintained under non-differentiating medium and refreshed every 2 days for the remaining of the experiment. After 48 h treatment, the medium was changed to differentiating medium [DMEM (high glucose) containing 10% FBS, 100 U/mL penicillin, 100 mg/mL streptomycin and 10 μg/mL insulin]. The experiment was terminated on day 7-10. Cells were washed with PBS x2 and fixed with 10% formaldehyde in PBS for 1 h at RT. Subsequently, the cells were washed with propylene glycol (85% (v/v) and air dried. Oil Red O (ORO) staining and gene markers were used to document the progression of differentiation and adipogenesis. Working solutions of fresh ORO (0.5%, cat# 26609-01, Electron Microscopy Sciences) were prepared by diluting with distilled water in the ratio of 6:4, followed by incubation for 20 min and filtration (0.2 μm). ORO working solution (1.5 mL) was added to each well and incubated in the dark for 1 h. The wells were washed with distilled water, dried, and photographed using an inverted microscope (magnification of 4× or 10×) with universal infinity-corrected optics (UIS2), a 6V/30W halogen bulb, an ultra-long working distance condenser (N.A. 0.3, W.D. 72 mm) and an Olympus U-LS30-3 camera.

Images were processed by using Infinity Capture Software Version 6.5.4. ORO staining was either relatively quantified or cells were counter-stained with hematoxylin, leading to shown representative image (Figure S9, Supporting Information). The ORO stain was extracted with isopropanol (500 µl per well/ 6-well plate) using proper controls to substract background. The absorbance was measured at 462 nm using a SpectraMax 5M spectrometer and data plotted.

Preadipocyte Differentiation Assay. Poietics™ human visceral (Cat# PT-5005, Lonza) or subcutaneous (Cat# PT-5020, Lonza) human preadipocytes were cultured and expanded according to the manufacturer's protocol. The preadipocyte cell batches were used up to passage 3 and maintained with fibroblast basal medium (ATCC® PCS-201-030, 5% FBS, 1% Pen/Strep, 1% GlutaMAX™, rh FGF β (5 ng/mL), ascorbic acid (50 µg/mL), hydrocortisone hemisuccinate (50 µg/mL), insulin 1 µg/mL) and refreshed every 3-4 days after plating. These cells have a doubling time of 34-44 h based on batch. Cell viability was measured routinely by trypan Blue exclusion assay (Cat. 315250061) using a cellometer (Nexcelom AutoT4). Preadipocytes were cultured to 70% confluency, and then plated for the differentiation assay. The adipocyte differentiation ToolKit ATCC PCS-500-050 was followed according to the manufacturer's instructions. Briefly, cells were resuspended in preadipocyte medium and plated at 100,000 cells/well in 6-well culture plates in 1.5 mL of preadipocyte growth medium. Incubated at 37 °C, 5% CO_2, and > 90% humidity until confluency. On day 0, the media was removed, and induction medium with or without hydrocortisone hemisuccinate (50 µg/mL) was added, treated with vehicle (DMSO 0.2%), rosiglitazone (2 µM) or CA (50, 100 µM). Non-differentiation medium (NDM) was used for non-differentiating control cells. After 48 h, the medium of the induced cells was changed to differentiation medium and treated with vehicle or CA. The media was refreshed every 48-72 h until assay completion (9-14 days). The extent of adipocyte differentiation was recorded by microscopic observation of lipid vacuoles in the induced cells. The intracellular lipid vacuoles began to

appear by day 4 and continue to increase in size and number. Non-induced cells had few, if any, lipid vacuoles. To document adipocyte differentiation, the cells were rinsed with PBS, fixed with 10% buffered formaldehyde for 1 h. The formaldehyde was discarded; the plates were rinsed twice with PBS and washed with propylene glycol (85% v/v) and then, stained with Poietics™ AdipoRed™ Reagent (PT-7009) or ORO stain. Representative images of a differentiation assay evaluating CA (50 μM) with ORO and hematoxylin stains are shown at 4× and 10× magnification (Figure S11, Supporting Information).

Quantitative Reverse Transcriptase Polymerase Chain Reaction (qRT-PCR). Total RNA was extracted by using Trizol (Invitrogen, Carlsbad, CA, USA). RNA quality was assessed via a 2100 Bioanalyzer (Agilent, Santa Clara, CA) and cDNA was synthesized with SuperScript III cDNA synthesis kit (Invitrogen, Carlsbad, CA, USA). All qPCR primers (Table S5) and SYBR Green Master Mix were purchased from (Qiagen, Valencia, CA). The qPCR reaction was performed by using an Applied Biosystems 17900 instrument (Applied Biosystems, Foster City, CA) and Life Technologies (Grand Island, NY). Relative expression levels were calculated by using the comparative C_T method ($\Delta\Delta C_T$) relative to the mean of 3 housekeeping genes (β-actin, PPIA and PPIB expression).[34]

Western Blot Analysis. Cell lysates were prepared with lysis buffer [10 mM Tris-HCl (pH 7.5), 100 mM NaCl, 1 mM EDTA, 1 mM EGTA, 1% (v/v) Triton X-100, 0.5% w/v) sodium deoxycholate, 0.1% (w/v) sodium dodecyl sulfate, and 10% (v/v) glycerol] supplemented with protease inhibitor cocktail (cOmplete™, and PhosSTOP™, Roche). Cell lysates were then centrifuged at 17000 g for 5 min at 4 °C. The soluble fraction was collected, and the protein concentration was determined via Pierce BCA protein assay (ThermoFisher Scientific, Grand Island, NY, USA). Total protein lysate (30 μg per lane) were separated by gel electrophoresis (SDS-PAGE) on 4%-12% BisTris-NuPage polyacrylamide gels using 1x MES as running buffer (ThermoFisher Scientific, Grand Island, NY, USA), transferred to

nitrocellulose membranes (0.22 μM pore size, LI-COR Biosciences) blocked with 5% nonfat dry milk, and the membranes were probed with the following monoclonal or polyclonal primary antibodies according to the manufacturer's recommendations. Membranes were then incubated overnight at 4 °C with antibodies specific for HSD11B1, PPARα (GenTex #s GTX104626 and GTX101098, respectively), PPARγ, PGC-1α (Abcam# ab191407 and ab54481, respectively), and GR (Cell Signaling #3660). Then, membranes were incubated with secondary antibodies (goat anti-rabbit-IgG labelled with IR-Dye 680RD or goat anti-mouse-IgG labelled with IR- Dye800CW [(LI-COR Biosciences, Lincoln, NE, USA), at a dilution of 1:15000, scanned and bands quantitated with a LI-COR Odyssey CLX system (LI-COR Biosciences, Lincoln, NE, USA).

Nascent Protein Synthesis Assay. Biovision's EZClick™ protein synthesis kit # K715-100 was conducted according to manufacturer's protocol. Normal mouse fibroblast (ATCC: CRL-2907) cells were plated at 2×10^4 per well in 8 well 1% gelatin coated ibidi μ-slides (80826) and incubated at 37 °C for 12 h in phenol red–free IMDM medium supplemented with 10% FBS. The cells were treated with CA (50 μM) for 2 h before click reaction, along with DMSO controls. Cycloheximide (20 nM) was used as a positive control and added 30 min prior to click reaction and staining protocol. Images shown were taken with a Nikon C2 point-scanning confocal microscope at 20× magnification and whole image montage was quantified with Gen5 3.04 Software (Winooski, VT, USA).

Human Glucocorticoid Receptor (GR) Reporter Assay. The cell line model MDA-MB-231 (ATCC® HTB-26) were transiently transfected with GR response element–driven luciferase DNA construct GoClone reporter vector S900015 or negative control reporter construct S790001 (Switchgear Genomics, Menlo Park CA), according to SwitchGear's protocols.[46] Lipofectin reagent (Gibco BRL/Invitrogen) was used according to the manufacturer's instructions. GRE: Luc cells (5000 cells/well) were seeded in 96-well plates (White plate #6005680, PerkinElmer) and incubated at 37 °C

for 12 h. Then, the medium was replaced by phenol red–free DMEM medium containing 2% charcoal-stripped FBS. The cells were treated with 100 nM dexamethasone, 50 μM CA or DMSO vehicle for 4 h. Then, LightSwitch luciferase assay reagent was added according to the manufacturer's protocol, and he signal was measured by using EnVision (PerkinElmer, Waltham, MA) and analyze with Graphpad Prism Software Version 7.02.

Human PPARγ Reporter Antagonist Assay. GeneBlazer® Flurorescence Resonance Energy Transfer Technology PPARγ–UAS-*bla* 293H cell-based assay system (Cat# K1701, invitrogen) was used following the manufacturer's protocol at 37 °C and 5% CO_2.[40] Cells were plated (18,000 cells/ well) in poly-D-lysine–coated 384-well Microtest™ Plates (BD BioCoat REF356663) in 32 μL of phenol red–free DMEM medium supplemented with 2% charcoal-stripped FBS, penicillin (100 U/mL), and streptomycin (100 μg/mL). The assay plates were incubated for 6 h, then treated with test compounds in a dose response format (covering 10 concentrations, ranging from 40 μM to 2 nM). After 30 min incubation, rosiglitazone was added, yielding a final concentration of 20 nM per well. The assay plate was incubated for 16 h, treated with the manufacturer's lysis buffer, followed by 8 μL of 6X substrate mixture, and incubated at RT for 2 h in the absence of light. Then, the signal was measured by using a multilabel reader EnVision (PerkinElmer, Waltham, MA) equipped with an excitation filter of 400 nm with a bandwidth of 25 nm, a first emission filter of 535 nm with a bandwidth of 25 nm, a second emission filter of 460 nm with a bandwidth of 25 nm, and a dichroic filter with a cutoff of 425 nm.

Mitochondria Evaluation by Confocal Microscopy. For lipid and mitochondria staining 3T3-L1 cells were seeded in 8-well chambers (ibidi μ-slides #80826) and the adipogenesis assay was conducted as described above. On day 7, the cells were washed were stained with MitoTracker® Red at 50 nM for 30 min, washed with PBS and treated with 4% formaldehyde (100 uL per well) for 30 min at RT. The

cells were washed and treated with HCS LipidTOX™ Green neutral staining (1X solution). After 30 min at RT, the cells were washed and imaged on a 3i Marianas Spinning Disk confocal microscope system at 63x magnification (Figure S16, Supporting Information). After imaging, the intensity of green stain was quantified using the Slide Viewer software package 6. For live-cell imaging, 3T3-L1 cells were seeded in 8-well ibidi chambers and the adipogenesis assay was conducted as described above. On day 7, live 3T3-L1 cells were stained with MitoTracker® Deep Red to a final concentration of 50 nM and Hoechst 33342, washed with PBS and imaged on a 3i Marianas spinning disk confocal imaging system configured with Yokagoma CSU-X spinning disk scanhead. For each field of view an image stack consisting of 30 optical sections was taken at 63× magnification. Images represent a single optical section for each field of view. Averages of the mean intensity for each group were calculated and plotted.

Data Analysis. Statistical differences and standard error of the mean (S.E.M.) between 2 groups were analyzed by using Student's two-tailed *t*-test. For comparison of multiple samples, statistical analysis was performed by using ANOVA's one-way non-parametric test followed by Dunnett's multiple comparison post-test or Tukey's test. P values < 0.05 were considered statistically significant. For CTG, the mean luminescence of each experimental treatment group was normalized as a percentage of the mean intensity of untreated controls. EC_{50} values (μM) were calculated by Pipeline Pilot Software (Accelrys, Enterprise Platform, CA, USA) or GraphPad Prism 7.0 (GraphPad Prism Software Inc., San Diego, CA, USA).

ASSOCIATED CONTENT

Supporting Information

The Supporting Information is available free of charge on the ACS Publications website at DOI:

X-ray data collection and refinement statistics for **1**; evaluation of **1** and analogues in proliferation assay, in vitro ADME and preliminary in vivo PK analysis of **1**; evaluation of 11β-HSD1 and 2 graphs; ^{1}H NMR and ^{13}C NMR spectra (Figures S17-S84) and mass spectra data of compounds *ent*-**1**, **4**-**20**, and key intermediates (PDF). Molecular formula strings (CSV)

Accession Codes

PDB code for **1** is 6NJ7. Authors will release the atomic coordinates and experimental data upon article publication.

AUTHOR INFORMATION

Corresponding Author

* Tel: 901-595-6504. E-mail: Fatima.rivas@stjude.org

Author Contributions

The manuscript was written through contributions of all authors. All authors have given approval to the final version of the manuscript.

ORCID

Fatima Rivas: 0000-0003-3643-2035

Notes

The authors declare no competing financial interests.

ACKNOWLEDGMENTS

The study was supported by ALSAC St Jude Children's Research Hospital. X-ray data were collected at Southeast Regional Collaborative Access Team (SER-CAT) 22-ID beamline at the Advanced Photon Source, Argonne National Laboratory. Supporting institutions may be found at http://www.ser-cat.org/members.html. Use of the Advanced Photon Source was supported by the US Department of Energy, Office of Science, Office of Basic Energy Sciences, under Contract No. W-31-109-Eng-38. The authors thank the Analytical Technologies Center Core Facility, the Preclinical PK Shared Resource the Flow and Cell Cycle Facility, and the Cell and Tissue Imaging Center of St. Jude Children's Research Hospital. All centers were supported in part by the Cancer Center Support Grant (P30CA021765) from the U.S.A. National Cancer Institute, NIH, Bethesda, MD.

ABBREVIATIONS

CA, colletoic acid; 11β-HSD1, 11β-hydroxysteroid dehydrogenase type 1; GC, glucocorticoid; MetS, metabolic syndrome; T2DM, type 2 diabetes mellitus.

REFERENCES

(1) Granner, D. K.; Wang, J. C.; Yamamoto, K. R. Regulatory actions of glucocorticoid hormones: from organisms to mechanisms. *Adv. Exp. Med. Biol.* **2015**, *872*, 3-31.

(2) Harno, E.; White, A. Will treating diabetes with 11β-HSD1 inhibitors affect the HPA axis? *Trends Endocrinol. Metab.* **2010**, *21*, 619-627.

(3) Valsamakis, G.; Anwar, A.; Tomlinson, J. W.; Shackleton, C. H.; McTernan, P. G.; Chetty, R.; Wood, P. J.; Banerjee, A. K.; Holder, G.; Barnett, A. H.; Stewart, P. M.; Kumar, S. 11Beta-hydroxysteroid dehydrogenase type 1 activity in lean and obese males with type 2 diabetes mellitus. *J. Clin. Endocr. Met.* **2004**, *89*, 4755–4761.

(4) Seckl, J. R.; Morton, N. M.; Chapman, K. E.; Walker, B. R. Glucocorticoids and 11beta-hydroxysteroid dehydrogenase in adipose tissue. *Recent. Prog. Horm. Res.* **2004**, *59*, 359-393.

(5) (a) Tang, Q. Q.; Lane, M. D. Adipogenesis: from stem cell to adipocyte. *Annu. Rev. Biochem.* **2012**, *81*, 715−736. (b) Seckl, J. R.; Walker, B.R. Minireview: 11β-hydroxysteroid dehydrogenase type 1—a tissue-specific amplifier of glucocorticoid action. *Endocrinology* **2001**, *142*, 1371-1376. (c) Baum, E.; Zhang, W.; Li, S.; Cai, Z.; Holden, D.; Huang, Y. A novel 18F-labeled radioligand for positron emission tomography imaging of 11β-hydroxysteroid dehydrogenase (11β-HSD1): synthesis and preliminary evaluation in nonhuman primates. *ACS Chem. Neurosci.* 2019, *10*, 2450-2458.

(6) Gregoire, F. M. Adipocyte differentiation: from fibroblast to endocrine cell. *Exp. Biol. Med*. **2001**, *226*, 997−1002.

(7) Lehr, S.; Hartwig, S.; Sell, H. Adipokines: A treasure trove for the discovery of biomarkers for metabolic disorders. *Proteomics: Clin. Appl.* **2012**, *6*, 91−101.

(8) Paterson, J. M.; Seckl, J. R.; Mullins, J. J. Genetic manipulation of 11β-hydroxysteroid dehydrogenases in mice. *Am. J. Physiol. Regul. Integr. Comp. Physiol.* **2005**, *289*, R642–R652.

(9) Kotelevtsev, Y.; Holmes, M. C.; Burchell, A.; Houston, P. M.; Schmoll, D.; Jamieson, P.; Best, R.; Brown, R.; Edwards, C. R.; Seckl, J. R.; Mullins, J. J. 11β-Hydroxysteroid dehydrogenase type 1

knockout mice show attenuated glucocorticoid-inducible responses and resist hyperglycemia on obesity or stress. *Proc. Natl. Acad. Sci. U.S.A.* **1997**, *94*, 14924-14929.

(10) Stefan, N.; Ramsauer, M.; Jordan, P.; Nowotny, B.; Kantartzis, K.; Machann, J.; Hwang, J. H.; Nowotny, P.; Kahl, S.; Harreiter, J.; Hornemann, S.; Sanyal, A. J.; Stewart, P. M.; Pfeiffer, A. F.; Kautzky-Willer, A.; Roden, M.; Häring, H. U.; Fürst-Recktenwald, S. Inhibition of 11β-HSD1 with RO5093151 for non-alcoholic fatty liver disease: a multicentre, randomised, double-blind, placebo-controlled trial. *Lancet Diabetes Endocrinol.* **2014**, *2*, 406-416.

(11) Freude, S.; Heise, T.; Woerle, H. J.; Jungnik, A.; Hamilton, B.; Schölch, C.; Huang, F.; Graefe-Mody, U. Safety and pharmacodynamics of BI 135585, a selective inhibitor of 11β-hydroxysteroid dehydrogenase-1 (HSD1) in humans: liver and adipose tissue 11β-HSD1 inhibition after acute and multiple administration over 2 weeks. *Diabetes Obes. Metab.* **2016**, *18*, 483-490.

(12) (a) Feig, P. U.; Shah, S.; Hermanowski-Vosatka, A.; Plotkin, D.; Springer, M. S.; Donahue, S.; Thach, C.; Klein, E. J.; Lai, E.; Kaufman. K. D. Effects of an 11β-hydroxysteroid dehydrogenase type 1 inhibitor, MK-0916, in patients with type 2 diabetes mellitus and metabolic syndrome. *Diabetes Obes. Metab*. **2011**, 13, 498–504. (b) Sundbom, M. M.; Kaiser, C.; Björkstrand, E.; Castro, V. M.; Larsson, C.; Selén, G.; Nyhem, C. S.; James, S. R. Inhibition of 11β-HSD1 with the S-phenylethylaminothiazolone BVT116429 increases adiponectin concentrations and improves glucose homeostasis in diabetic KKA^{y} mice. *BMC Pharmacol.* **2008**, *8,* 3-13.

(13) (a) Courtney, R.; Steward, P. M.; Toh, M.; Ndongo, M. N.; Calle, R. A.; Hirshberg, B. Modulation of 11beta-hydroxysteroid dehydrogenase type 1 activity biomarkers and pharmacokinetics of PF-00915275, a selective 11beta-HSD1 inhibitor. *J. Clin. Endocrinol. Metab.* **2008**, *93*, 550-556. (b) Nair, S. K.; Matthews, J. J.; Cripps, S. J.; Cheng, H.; Hoffman, J. E.; Smith, C.; Kupchinsky, S.; Siu, M.; Taylor, W. D.; Wang, Y.; Johnson, T. O.; Dress, K. R.; Edwards, M.

P.; Zhou, S.; Hosea, N. A.; Lapaglia, A.; Kang, P.; Castro, A.; Ermolieff, J.; Fanjul, A.; Vogel, J. E.; Rejto, P.; Dalvie, D. N-(Pyridin-2-yl) arylsulfonamide inhibitors of 11β-hydroxysteroid dehydrogenase type 1: strategies to eliminate reactive metabolites. *Bioorg. Med. Chem. Lett.* **2013**, *23*, 2344-2348.

(14) Scott, J. S.; Goldberg, F. W.; Turnbull, A. V. Medicinal chemistry of inhibitors of 11β-hydroxysteroid dehydrogenase type 1 (11β-HSD1). *J. Med. Chem.* **2014**, *57*, 4466-4486.

(15) (a) Newman, D. J.; Cragg, G. M. Natural products as sources of new drugs from 1981 to 2014. *J. Nat. Prod.* **2016**, *79*, 629-661. (b) Rodrigues, T.; Reker, D.; Schneider, P.; Schneider, G. Counting on natural products for drug design. *Nat. Chem.* **2016**, *8*, 531-541.

(16) Chen, X. Q.; Shao, L. D.; Pal, M.; Shen, Y.; Cheng, X.; Xu, G.; Peng, L.Y.; Wang, K.; Pan, Z. H.; Li, M. M.; Leng, Y.; He, J.; Zhao, Q. S. Hupehenols A-E, selective 11β-hydroxysteroid dehydrogenase type 1 (11β-HSD1) inhibitors from viburnum hupehense. *J. Nat. Prod.* **2015**, *78*, 330-334.

(17) Chapman, K.; Holmes, M.; Seckl, J. 11β-Hydroxysteroid dehydrogenases: intracellular gate-keepers of tissue glucocorticoid action. *Physiol Rev.* **2013**, *93*(3), 1139-1206.

(18) Aoyagi, A.; Ito-Kobayashi, M.; Ono, Y.; Furukawa, Y.; Takahashi, M.; Muramatsu, Y.; Umetani, M.; Takatsu, T. Colletoic acid, a novel 11β-hydroxysteroid dehydrogenase type 1 inhibitor from *Colletotrichum gloeosporioides* SANK 21404. *J. Antibiot.* **2008**, *61*, 136–141.

(19) Ling, T.; Griffith, E.; Mitachi, K.; Rivas, F. Scalable and divergent total synthesis (+)-colletoic acid, a selective 11β-hydroxysteroid dehydrogenase type 1 inhibitor. *Org. Lett*. **2013**, *15*, 5790–5793.

(20) Ling, T.; Gautam, L. N.; Griffith, E.; Das, S.; Lang, W.; Shadrick, W. R.; Shelat, A.; Lee, R.; Rivas, F. Synthesis and evaluation of colletoic acid core derivatives. *Eur. J. Med. Chem.* **2016**, *110*, 126-132.

(21) Su, X.; Vicker, N.; Potter, B. V. L. Inhibitors of 11beta-hydroxysteroid dehydrogenase type 1. *Prog. Med. Chem.* **2008**, *46*, 29-130.

(22) Hosfield, D. J.; Wu, Y.; Skene, R. J.; Hilgers, M.; Jennings, A.; Snell, G. P.; Aertgeerts, K. Conformational flexibility in crystal structures of human 11beta-hydroxysteroid dehydrogenase type 1 provide insights into glucocorticoid interconversion and enzyme regulation. *J. Biol. Chem.* **2005**, *280*, 4639-4648.

(23) Xu, R.; Sang, B. C.; Navre, M.; Kassel, D. B. Cell-based assay for screening 11beta-hydroxysteroid dehydrogenase inhibitors using liquid chromatography/tandem mass spectrometry detection. *Rapid Commun. Mass Spectrom.* **2006**, *20*, 1643–1647.

(24) Thomas, M. P.; Potter, B. V. L. Crystal structures 11β-hydroxysteroid dehydrogenase type 1 and their use in drug discovery. *Future Med. Chem*. **2011**, *3*, 367-390.

(25) Esteves, C. L.; Kelly, V.; Begay, V.; Man, T. Y.; Morton, N. M.; Leutz, A.; Seckl, J. R.; Chapman, K. E. Regulation of adipocyte 11β-hydroxysteroid dehydrogenase type 1 (11β-HSD1) by CCAAT/enhancer-binding protein (C/EBP) β isoforms, LIP and LAP. *PLoS ONE* **2012**, *7*, e37953.

(26) Yang, Z.; Guo, P.; Zhu, W.; Li, L.; Myatt, K.; Sun, J. Role of glucocorticoid receptor and CCAAT/enhancer-binding protein in the feed-forward induction of 11beta-hydroxysteroid dehydrogenase type 1 expression by cortisol in human amnion fibroblasts. *J. Endocrinol.* **2007**, *195*, 241–253.

(27) Li, X.; Kim, J. W.; Grønborg, M.; Urlaub, H.; Lane, M. D.; Tang, Q. Q. Role of cdk2 in the sequential phosphorylation/activation of C/EBPbeta during adipocyte differentiation. *Proc. Natl. Acad. Sci. U.S.A.* **2007**, *104*, 11597–11602.

(28) Muir, L. A.; Baker, N. A.; Washabaugh, A. R.; Neeley, C. K.; Flesher, C. G.; DelProposto, J. B.; Geletka, L. M.; Ghaferi, A. A.; Finks, J. F.; Singer, K.; Varban, O. A.; Lumeng, C. N.; O'Rourke, R.W. Adipocyte hypertrophy-hyperplasia balance contributes to weight loss after bariatric surgery. *Adipocyte* **2017**, *6*, 134-140.

(29) Coelho, M.; Oliveira, T.; Fernandes, R. Biochemistry of adipose tissue: an endocrine organ. *Arch. Med. Sci.* **2013**, *9*, 191-200.

(30) Granner, D. K.; Wang, J. C.; Yamamoto, K. R. Regulatory actions of glucocorticoid hormones: from organisms to mechanisms. *Adv. Exp. Med. Biol.* **2015**, *872*, 3-31.

(31) Rutkowski, J. M.; Stern, J. H.; Scherer, P. E. The cell biology of fat expansion. *J. Cell Biol.* **2015**, *208*, 501–512.

(32) Napolitano, A.; Voice, M. W.; Edwards, C. R. W.; Seckl, J. R., Chapman, K. E. 11Beta-hydroxysteroid dehydrogenase 1 in adipocytes: expression is differentiation-dependent and hormonally regulated. *J. Steroid. Biochem. Molec. Biol.* **1998**, *64*, 251-260.

(33) (a) Kim, J.; Temple, K. A.; Jones, S. A.; Meredith, K. N.; Basko, J. L.; Brady, M. J. Differential modulation of 3T3-L1 adipogenesis mediated by 11beta-hydroxysteroid dehydrogenase-1 levels. *J. Biol. Chem.* **2007**, *282*, 11038-11046. (b) Zebisch, K.; Voigt, V.; Wabitsch, M.; Brandsch, M. Protocol for effective differentiation of 3T3-L1 cells to adipocytes. *Anal. Biochem.* **2012**, *425*, 88-90.

(34) Mehlem, A.; Hagberg, C. E.; Muhl, L.; Eriksson, U.; Falkevall, A. Imaging of neutral lipids by oil red O for analyzing the metabolic status in health and disease. *Nat. Protoc.* **2013**, *8*, 1149-1154.

(35) (a) Fox, K. E.; Colton, L. A.; Erickson, P. F.; Friedman, J. E.; Cha, H. C.; Keller, P.; MacDougald, O. A.; Klemm, D. J. Regulation of cyclin D1 and Wnt10b gene expression by cAMP-responsive element-binding protein during early adipogenesis involves differential promoter methylation. *J. Biol. Chem.* **2008**, *283*, 35096–35105. (b) Pfaffl, M. W.; Tichopad, A.; Prgomet, C.; Neuvians, T. P. Determination of stable housekeeping genes, differentially regulated target genes and sample integrity: BestKeeper – excel-based tool using pair-wise correlations. *Biotechnol. Lett.* **2004**, *26*, 509-515.

(36) Balachandran, A.; Guan, H.; Sellan, M.; Vanuum, S.; Yang, K. Insulin and dexamethasone dynamically regulate adipocyte 11beta-hydroxysteroid dehydrogenase type 1. *Endocrinology* **2008**, *149*, 4069–4079.

(37) (a) Kelly, T. J.; Lerin, C.; Haas, W.; Gygi, S. P.; Puigserver, P. GCN5-mediated transcriptional control of the metabolic coactivator PGC-1beta through lysine acetylation. *J. Biol. Chem.* **2009**, *284*, 19945-19952. (b) Kubota, N.; Terauchi, Y.; Miki, H.; Tamemoto, H.; Yamauchi, T.; Komeda, K.; Satoh, S.; Nakano, R.; Ishii, C.; Sugiyama, T.; Eto, K.; Tsubamoto, Y.; Okuno, A.; Murakami, K.; Sekihara, H.; Hasegawa, G.; Naito, M.; Toyoshima, Y.; Tanaka, S.; Shiota, K.; Kitamura, T.; Fujita, T.; Ezaki, O.; Aizawa, S.; Kadowaki, T. PPAR gamma mediates high-fat diet-induced adipocyte hypertrophy and insulin resistance. *Mol. Cell.* **1999**, *4*, 597-609.

(38) Iwabu, M.; Yamauchi, T.; Okada-Iwabu, M.; Sato, K.; Nakagawa, T.; Funata, M.; Yamaguchi, M.; Namiki, S.; Nakayama, R.; Tabata, M.; Ogata, H.; Kubota, N.; Takamoto, I.; Hayashi, Y. K.; Yamauchi, N.; Waki, H.; Fukayama, M.; Nishino, I.; Tokuyama, K.; Ueki, K.; Oike, Y.; Ishii, S.; Hirose, K.; Shimizu, T.; Touhara, K.; Kadowaki, T. Adiponectin and AdipoR1 regulate PGC-1α and mitochondria by Ca(2+) and AMPK/SIRT1. *Nature* **2010**, *464*, 1313-1319.

(39) Liu, J.; Xu, Y.; Stoleru, D.; Salic, A. Imaging protein synthesis in cells and tissues with an alkyne analog of puromycin. *Proc. Natl. Acad. Sci. U.S.A.* **2012**, *109*, 413-418.

(40) Meijsing, S. H.; Pufall, M. A.; So, A. Y.; Bates, D. L.; Chen, L.; Yamamoto, K. R. DNA binding site sequence directs glucocorticoid receptor structure and activity. *Science* **2009**, *324*, 407-410.

(41) (a) Tsukahara, T. The role of PPARγ in the transcriptional control by agonists and antagonists. *PPAR Research* **2012**, 1-9. (b) Chin, J.; Adams, A. D.; Bouffard, A.; Green, A.; Lacson, R. G.; Smith, T.; Fischer, P. A.; Menke, J. G.; Sparrow, C. P.; Mitnaul, L. J. Miniaturization of cell-based β-lactamase depedent FRET assays to ultra-high throughput formats to identify agonists of humal liver X receptors. *Assay and Drug Dev. Tech*. 1, **2003**, 777-787. (c) Ma, J. J.; Zhang, T.; Fang, N.; Zou, Y.; Gong, Q. H.; Yu, L. M.; Chen, D. X. Establishment of a cell-based drug screening model for identifying agonists of human peroxisome proliferator-activated receptor gamma (PPARγ). *J. Pharm. Pharmacol.* **2012**, *64*, 719-726.

(42) Ling, T., Lang, W. H.; Martinez-Montemayor, M. M.; Rivas, F. Development of ergosterol peroxide probes for cellular localisation studies. *Org. Biomol. Chem.* **2019**, 17 (21), 5223-5229.

(43) McCoy, A. J.; Grosee-Kunstleve, R. W.; Adams, P. D.; Winn, M. D.; Storoni, L. C.; Read, R. J. Phaser crystallographic software. *J. Appl. Crystallogr.* **2007**, *40*, 658–674.

(44) (a) Emsley, P.; Cowtan, K. Coot: model-building tools for molecular graphics. *Acta Crystallogr. D Biol. Crystallogr.* **2004**, *60*, 2126–2132. (b) Chen, V. B.; Arendall, W. B.; Headd, J. J.; Keedy, D. A.; Immormino, R. M.; Kapral, G. J.; Murray, L. W.; Richardson, J. S.; Richardson, D. C. MolProbity: all-atom structure validation for macromolecular crystallography. *Acta Crystallogr. D Biol. Crystallogr.* **2010**, *66*, 12–21.

(45) DeLano, W. L. The PyMOL molecular graphics system. **2002**, *DeLano Scientific, Palo Alto, CA*.

(46) Zhang, J.; Chalmers, M. J.; Stayrook, K. R.; Burris, L. L.; Wang, Y.; Busby, S.A. Pascal, B. D.; Garcia-Ordonez, R. D.; Bruning, J. B.; Istate, M. A.; Kojetin, D. J.; Dodge, J. A.; Burris, T. P.; Griffin, P. R. DNA binding alters coactivator interaction surfaces of the intact VDR-RXR complex. *Nat. Struct. Mol. Biol.* **2011**, *18*, 556–563.

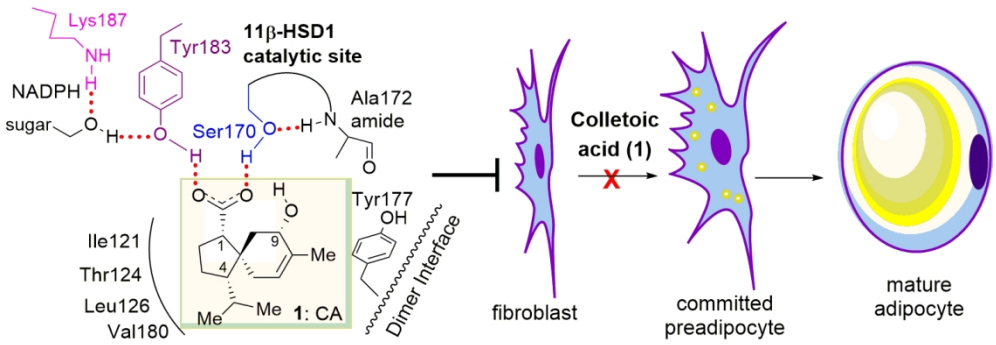

134x46mm (300 x 300 DPI)